KU LEUVEN

FACULTEIT INGENIEURSWETENSCHAPPEN

Current and state-of-the-art techniques for high dynamic range

Dries Kerkhofs

Thesis submitted for the degree of
Master of Science in
Electrical Engineering, ec

Thesis supervisors:
Prof. dr. ir. Filip Tavernier
Prof. dr. Trond Ytterdal

Assessors:
Prof. dr. ir. George Gielen
Prof. dr. ir. Tinne Tuytelaars

Mentors:
Ing. Arno Van Hoorebeeck
Ing. Gerlinde Ruttens

Academic year 2021 – 2022

Master of Science in Electrical Engineering

Preface

As I finish the final steps of my training at KU Leuven, I would like to acknowledge the people who helped me realize this master's thesis:

First and foremost, I would like to thank my supervisors Arno Van Hoorebeeck and Gerlinde Ruttens at Caeleste for their guidance and willingness to answer my questions about the topic and beyond. Their involvement has been indispensable for the completion of this project. Also many thanks to the company and the people of Caeleste for opening their doors for me and offering me the opportunity to be a part of a professional enterprise putting theory into practice. It has been an extraordinary enriching experience.

At KU Leuven I want to express my special thanks of gratitude to my promotor prof. Filip Tavernier for all the help and feedback sessions he offered me during this academic year. I would also like to thank prof. George Gielen and prof. Tinne Tuytelaars for making the time to evaluate the thesis.

Also an expression of gratitude towards prof. Trond Ytterdal of NTNU, for enabling the combination of a dissertation and an international academic experience. It's been interesting seeing the methods of Norway's top engineering university up close.

Finally I would like to thank my family, friends and partner for supporting me during these last 5 years.

Dries Kerkhofs

Contents

Abstract

High dynamic range (HDR) image sensors often produce multiple frames that have to be combined into one image. The goal of this research is to synthesize an HDR image from the frames produced by state-of-the-art HDR image sensors. To do this, a correction of the frames has to be done first. A calibration based method is used, because this produces the most accurate and predictable results. A photoresponse measurement and dark current measurement are required to find the required calibration parameters. The proposed method is optimized for image sensors produced at Caeleste. The dominant noise sources are identified first, and then corrected in the order in which they occur. A polynomial non-linearity correction for each pixel separately is implemented, and the dark current is estimated based on the black pixels to make the correction drift resistant. A method is proposed in this thesis to optimally merge the frames to achieve a good SNR over the dynamic range, while also limiting the artefacts. Finally, the proposed methods have been tested on real image sensors, while operating these sensors in different modes. The algorithm was able to successfully reduce the non-uniformities and merge the frames.

List of Figures and Tables

List of Figures

List of Tables

List of Abbreviations and Symbols

Abbreviations

ADC	Analog digital converter
CDS	Correlated double sampling
CCD	Charge coupled device
CIS	CMOS image sensor
CVF	Charge-to-voltage conversion factor
EHP	Electron hole pair
FD	Floating diffusion
FPN	Fixed Pattern noise
FWC	Full well capacity
HDR	High dynamic range
IWR	Integrate while read
NL	Non-linearity
PD	Photodiode
PPD	Pinned photodiode
SCR	Space charge region
SNR	Signal-to-noise ratio
TG	Transfer gate

Symbols

A	Ampere
C	Capacitance
I_{dark}	Dark current
I_{ph}	Photocurrent
k	Boltzmann constant
L_x	Illuminance
Q	Charge
q	Charge of an electron
T	Temperature
t	Integration time
V	Voltage
σ_x	Noise source
μ_x	Mean

Chapter 1

Introduction

The image sensor market has grown a lot over the last years. It currently has a 4.7% market share in the global semiconductor market and is predicted to keep growing in the next years [7]. Dynamic range is an important characteristic for image sensors. It represents the ability to capture a scene that has both dark and well illuminated parts at the same time. This is required in many applications, ranging from mobile phones to self-driving cars. However, in conventional linear pixel architectures, the dynamic range is limited by the noise.

CMOS image sensors have traditionally been more popular than charge coupled devices in consumer applications because of their lower price. Additionally, in recent years they have also been growing in importance in high performance applications (space, medical, ... applications). These CMOS image sensors give designers the option to add extra transistors to each pixel and use this freedom to increase the dynamic range. Often, these techniques result in a sensor that produces multiple frames instead of just one high-dynamic-range image. The output of these sensors then has to be processed and combined to generate the HDR image. This thesis will investigate the state-of-the-art HDR sensors currently in use and develop a post-processing algorithm for these sensors. The focus will be on high-performance image sensors instead of consumer cameras. The information contained in the HDR image will thus be a more important metric than the "beauty" of the images.

1.1 Thesis Organization

The next chapter is an introduction to image sensors and their properties. All the concepts required to understand the rest of this thesis will be explained here. Chapter three gives an overview of the HDR sensors currently in use and discusses their advantages and disadvantages. Chapter four proposes an image correction algorithm to remove the spatial noise and to linearise the image sensor. This is required before the HDR frames can be merged. Chapter five will then discuss a method to merge the frames outputted by an HDR image sensor into one image. Finally, the proposed methods are tested on two real image sensors, both with a different pixel architecture.

Chapter five and six will show the results of the measurements that have been done and verify the performance of the proposed algorithm on both of the sensors.

1.2 Caeleste

This thesis was done in collaboration with Caeleste. They are a fabless image sensor design company in Mechelen which focuses on sensors for medical, space or industrial applications. They are responsible for both the design and characterization of new sensors, and provided access to their lab, image sensors and knowledge for the research.

Chapter 2

Image Sensor Concepts

This chapter provides the reader with background information about image sensors. The basic operation principles of an image sensor will be explained first. Afterwards, an overview of the static and temporal noise sources in an image sensor is given. Some other performance metrics of CMOS image sensors will be discussed as well. Finally, the chapter ends with a detailed study about the dynamic range and signal-to-noise-ratio (SNR).

2.1 Light

The main purpose of a digital image sensor is to transform light intensity to digital data fit for computer representation, ideally with the lowest amount of noise and offset possible. It is therefore important to first look at some basic properties of light.

Each object has an illuminance and an emittance. The illuminance is the amount of light received by an object. The S.I. unit of this is lux or $lumens/m^2$. This unit is weighted to match the perceived light intensity observed by the human eye. Because this weighting is not useful for image sensors, which sometimes even operate outside the visible light range. The unit of W/m^2 at the frequency of the light source is used for the rest of this thesis as the unit for illuminance. An object can also emit light (on its own or because of reflections), called emittance. For the same reason as for the illuminance, the unit used in this thesis will be $watt$ instead of lux. There can be a huge difference in light intensities in nature, ranging from an illuminance of around $1000W/m^2$ of white light outdoors in the sunlight to around $1W/m^2$ in a normally illuminated office and even lower in night conditions [18]. An image sensor is often required to capture details in both dark and bright spots in a scene, both in good and poor lightning conditions, thus requiring a large dynamic range.

A large dynamic range is however not always required. An image sensor can also change its light sensitivity between scenes (called interscene dynamic range), for example by changing the integration time. Only when a scene itself contains a large

difference in illuminance is the image sensor required to have a large dynamic range as well (intrascene dynamic range) [18].

The human eye has a dynamic range of around 120 dB [16]. A linear image sensor designed to have the same dynamic range would thus require an output accuracy of at least 20 bits, which is very difficult to design with analog electronics because of the noise, mismatch and distortion limitations in analog circuits. Because of these limitations, it is in some cases necessary to design specialized high dynamic range image sensors.

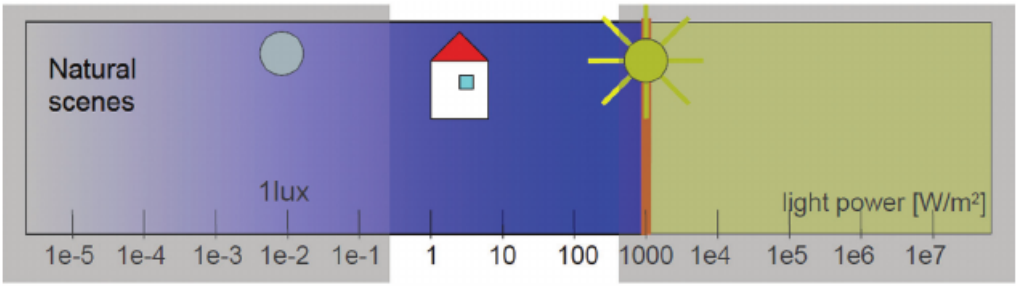

Figure 2.1: Comparison between the illuminance occurring in natural scenes VS the illuminance of a low dynamic range image sensor. Courtesy [18].

.

2.2 Photodetectors

The most common way to transform the incoming light to an electrical charge is using a PN photodiode (PD). When a photon with enough energy hits a silicon crystal, an electron hole pair (EHP) can be generated either by an intrinsic or extrinsic band-to-band transition [44]. Normally these EHPs would recombine quickly, but when the EHPs are generated in the space charge region (SCR) of a PN diode under reverse bias, the electric field in the space charge region will separate the optically generated electrons and holes. This results in an electrical current I_{ph}, called the photocurrent [44].

An improvement over the normal PN photodiode is the pinned photodiode (PPD). This photodiode has an extra grounded shallow highly doped P^+-layer between the oxide and the N-well implant of the PN diode (in the case of a P-type substrate) [16]. A schematic of a typical PPD is shown in figure 2.2a. The extra P^+-layer satisfies the dangling bonds at the $SI - SIO_2$ surface, reducing the dark current [24]. Another advantage of the PPD is that the n-well is fully depleted, resulting in a potential floor V_{pin} [52]. This means that when the PPD is connected to a lower potential well during read out, all the photo-generated electrons will be extracted from the PPD, resulting in ideally a complete readout and thus no image lag. This is illustrated in figure 2.2b. A mosfet acting as a switch, called the transfer gate

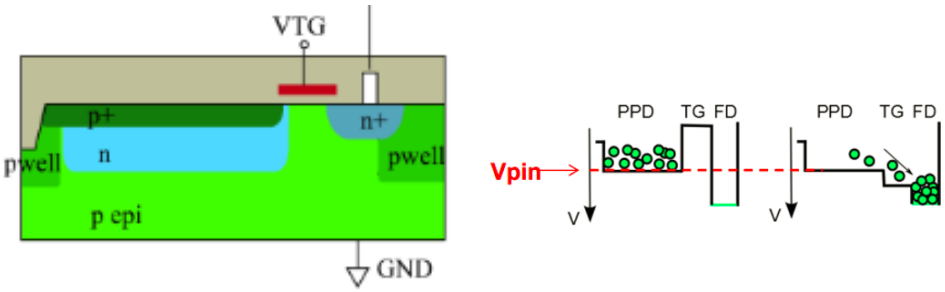

(A) schematic of a PPD showing the n-well, (B) Diagram showing the total charge P^+ implant and TG mosfet connecting the transfer from PPD to FD. Courtesy [42]. PPD to the FD. Courtesy [52].

FIGURE 2.2: Pinned photodiode.

(TG), is used for this purpose. This mosfet is typically created by reusing the N-well of the PN diode. In practice, there will always be some image lag (section 2.6.6).

2.3 Image Sensors

The photodiode as described in the previous section transforms a flux of photons into a flux of electrons (current). The most basic image sensor would thus be an array of these photodiodes where the current can be read out at the output for each pixel. It is however often more practical to first convert this current to a charge by doing an integration of the current over a certain time period (called integration time). Then this charge can be read out as a voltage instead. There are two important types of electronic image sensors: the charge coupled device (CCD) and the CMOS image sensor (CIS). Both devices can utilize the same types of photodetectors. The difference is how they read out the charge collected in each pixel.

2.3.1 Charge Coupled Devices

Charge coupled devices have been the most popular image sensor in the past and still remain dominant in some applications [14]. A CCD consists of an array of photodetectors and an analog shift register for readout. After an illumination period, the integrated charges are trapped in a potential well. As can be seen in figure 2.3, it is then possible to transport these charges by using a three phased clock to push the charges forward. The sensor is read out by first transferring the charges along a column towards the last row, and then transferring the charges along this row to an ADC. CCDs are today fabricated on specialized technology nodes, and often only the readout buffer is still fabricated on the same chip as the image sensor [24]. This often results in more expensive sensors, since a more expensive technology node and extra readout chips are needed, nevertheless with better overall performance (lower dark current and noise) [14]. The simpler pixel architecture also results in an increased fill factor (section 2.6.1) and a higher yield [24]. Today, CCDs still

dominate the large pixel image sensor market and are predicted to remain important in this sector in the near future [24].

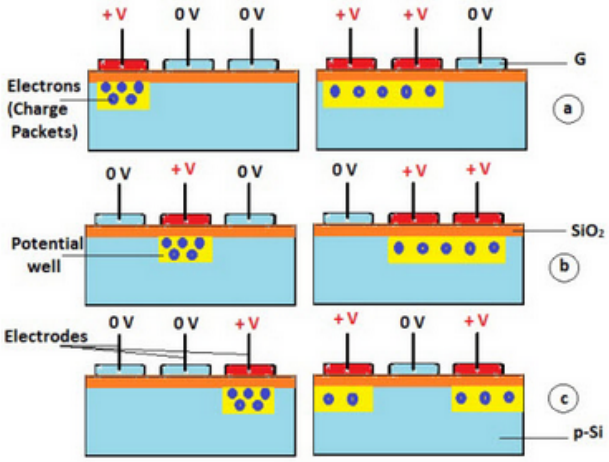

Figure 2.3: Method of charge transport in a CCD with a three phased clock to move charges to the next potential well. Courtesy [52].

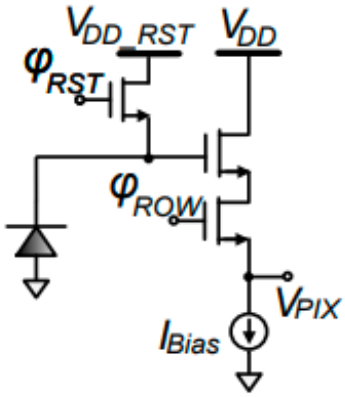

Figure 2.4: Schematic of a 3T pixel. Courtesy [30].

2.3.2 CMOS Image Sensors

CMOS image sensors are taking over the image sensor market at the moment. They can be implemented on standard CMOS technology, lowering their cost [52]. Because of this, most consumer electronics are currently CIS based. Furthermore, it is possible to implement other CMOS functionalities like ADCs or digital logic on the same chip, further reducing the cost of a camera system [14]. CMOS technology also offers the flexibility to add extra on-chip and even in-pixel functionality, for example HDR pixels. This extra flexibility in the readout chain can increase the frame rate of CIS compared to CCDs as well [14]. A basic 3T pixel structure can be seen in figure 2.4. The reset transistor is used to remove all the charge from the PN photodiode before every new image capture. During the integration, the photo generated charges are collected at the (parasitic) capacitor created by the photodiode and the pixel transistors connected to it. In an active pixel sensor (APS), this node is connected to a source follower to convert the charge to a voltage on the column wire. The source follower is also connected to a row select transistor. This transistor acts as a switch to select which pixel can be read out onto the column wire. Passive pixel sensors (PPS) do not have this source follower, this makes it difficult to read the charge on the high capacitive column wire. This makes PPS unpopular today.

A commonly used method to improve the pixel performance is the 4T pixel structure. This pixel makes use of the PPD described earlier instead of a normal PN photodiode. The charge is now first integrated on the PPD and then transferred to the node at the gate of the source follower (called the floating diffusion (FD)) by activating the TG.

This separation between the PPD and FD also allows to optimize the FD capacitance for optimal pixel gain and thus noise performance [25]. Another advantage of the 4T pixel is the possibility of correlated double sampling (CDS). The voltage on the FD before and after the integration are then read out. The sample before the integration includes the offsets and reset noise of the pixel, which can then be subtracted from the signal sample. This greatly reduces the kTC reset noise, 1/f noise and offset. More complex pixel architectures with more transistors are also used to improve for example global shutter performance, dynamic range or anti-blooming.

After the integration period, the voltages of all these pixels have to be read out and converted to a digital number. Each column of pixels is connected to a column wire. Using the row select transistors, all the pixels will be sequentially connected to the column wire and read out. A current source to drive the source followers of all the pixels is also connected to each column. The voltage on the column wire is typically buffered and then converted to a digital number by an ADC. These ADCs can be either on-chip or off-chip. It is also possible to use a single ADC to read out multiple columns to reduce the amount of ADCs needed. More complex readout circuits are possible depending on the required performance of the image sensor. Examples of these improvements are automatic CDS subtraction and pipelining for increased frame rate [34]. The readout method can be rolling shutter or global shutter. In rolling shutter, the pixels are read out immediately after integration row by row. This means that the integration period of all the rows does not begin and end at the same time, resulting in artefacts for fast moving objects, as can be seen in figure 2.5. In global shutter, all the pixels start their integration period at the same time and are then read out row by row. This means that the pixels need to be able to store the charge after integration. Inefficiencies in this charge storage can decrease the performance of global shutter image sensors [31].

(A) Rolling shutter. (B) Global shutter.

FIGURE 2.5: Artefacts in moving objects. Courtesy [4].

2.4 Temporal Noise in CMOS Pixels

Temporal noise causes the value of a pixel to vary between sequential frames when a pixel is under constant illumination. This noise limits the dynamic range in low light conditions because the signal will become indistinguishable from the noise. This section is a discussion of the dominant noise sources an a CMOS pixel. The overview below is mainly focussed on 4T pixels, although the same noise mechanisms are present in all CMOS pixels. The noise variance in the formulas in this chapter is expressed as the variation in the number of noise electrons.

2.4.1 Photon Shot Noise

This noise source is a shot noise or Poisson noise, meaning it is the result of the discrete nature of the photons hitting the photodetector [16]. The variance of the photon shot noise can be calculated as:

$$\sigma_{ph}^2 = \mu_{ph} = \frac{I_{ph} T_{int}}{q} \text{[24]} \tag{2.1}$$

Where μ_{ph} is the mean of the number of photo generated EHPs in the photodiode, I_{ph} is the photocurrent, T_{int} is the integration time and q is the charge of an electron. The photon shot noise is a physical limit to the SNR of an image sensor and is the dominant noise source when the illuminance on the sensor is large. To limit the photon shot noise (PSN) contribution compared to the total signal power, it is better to have a large amount of photo generated EHP. This can be done by for example increasing the integration time, quantum efficiency (section 2.6.2) or the pixel size.

2.4.2 Dark Current Shot Noise

Dark current shot noise is also a form of shot noise, but this time caused by the discrete nature of the dark current [24]. It can be described with the following formula:

$$\sigma_{dark}^2 = \frac{I_{dark} T_{int}}{q} \text{[26]} \tag{2.2}$$

Where I_{dark} is the dark current. To decrease this noise, the dark current should be minimized. This can for example be done by careful layout, using PPD based pixels or cooling the device [24]. A long integration time will also increase dark current shot noise. In a properly designed sensor, this DCSN is neglectable compared to the other noise sources [24].

2.4.3 Reset Noise

Reset noise is the variation of the charge on the floating diffusion (FD) capacitance after the resetting this capacitor through the reset transistor [16]. It is a thermal

noise source and it can be calculated as follows:

$$\sigma^2_{reset} = \frac{kTC_{fd}}{q^2}[16] \tag{2.3}$$

This noise can be greatly reduced by correlated double sampling.

2.4.4 Readout Noise

This noise is the result of all the noise added to the signal when the signal passes trough the readout chain. This can be all kinds of noise for example thermal noise or quantization noise. Sometimes, part of the readout is done off-chip (external ADC). The noise added there is also included in the readout noise for the scope of this thesis:

$$\sigma^2_{readout} = \frac{C^2_{fd}}{q^2}\overline{v^2_{readout}}[16] \tag{2.4}$$

Except by changing the source follower, the readout noise cannot be reduced at pixel level. Since this is mostly a thermal noise, it can also be reduced by operating the sensor at a lower temperature [2].

2.4.5 Flicker Noise

Flicker noise, also called 1/f noise or pink noise, is a noise inversely proportional to the frequency and is mostly generated at the gate of the source follower in a pixel [34]. It also depends on the mosfet gate area and is becoming more and more dominant in smaller technology nodes. The origin of flicker noise is not proven, but it is believed that it is generated by the trapping and releasing of charge carriers at the silicon and silicone-oxide interface at the gate of a mosfet [25]. CDS does help to reduce this, yet it remains an important contribution to the total noise [34] [36]. It can be reduced by increasing the size of the source follower or using a Pmos source follower [2].

2.4.6 Other Temporal Noise Sources

There are several other less dominant noise sources in an image sensor. For example clock feed-trough, noisy power supply, random telegraph noise [24] [2]. These noise sources will not be considered in this thesis, but added to the readout noise during the calculations.

2.5 Static Noise in CMOS Pixels

Static or spatial noise is the variation between the pixels in an image under constant illumination. This noise remains constant between images captured over time. This means that they can be compensated perfectly during post-processing (when there is enough characterization data available). However, this compensation is not always viable in practice because it can be computationally expensive or requires a lot of

characterization of each individual sensor. Some of these noise sources also depend on temperature or drift over time, making calibrating this even more difficult. CDS helps to reduce the static noise. This section discusses the most important fixed pattern noise sources for generic 4T pixel based image sensors.

2.5.1 Fixed Pattern Noise

Fixed Pattern noise (FPN) includes the variations in the signal between the pixels when there is no illumination and zero integration time. It is mainly the result of process variations and offset voltages, both on chip and externally in the case that some analogue processing happens off-chip. In figure 2.6, It is for example possible to see which columns were read out by the same ADC. The fixed pattern noise can be corrected by subtracting a dark frame from an image [24][16] [1]. Because FPN is added both in the pixel and in the readout chain, CDS will not always cancel this completely if it is done on-chip because it can still be introduced after the CDS operation.

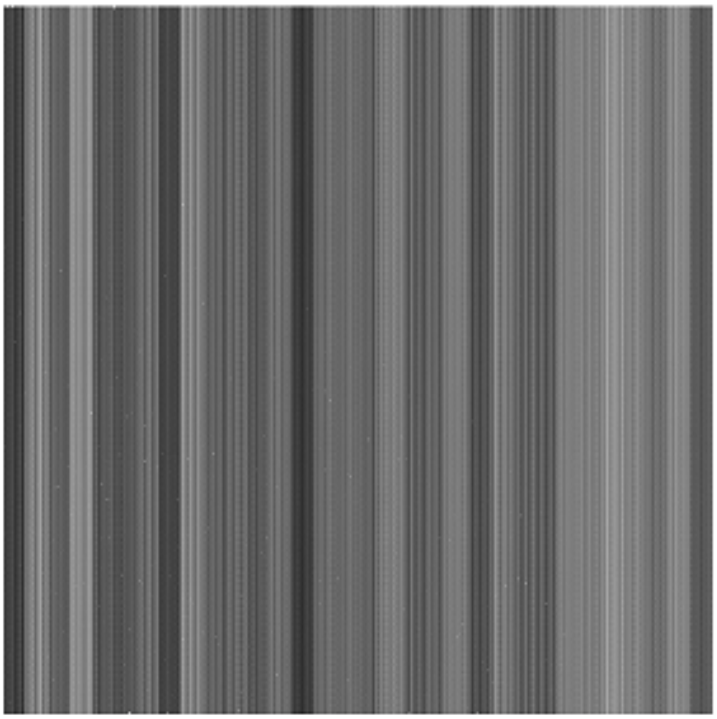

Figure 2.6: Dark image with increased contrast taken by a Caeleste image sensor that clearly shows which columns are read out by the same ADC.

2.5.2 Photoresponse Non-uniformity

The gain of all the pixels can be different as well because of a different capacitance of each storage node, photodiode area variations, doping variations, ... [2] This gives

rise to an illumination dependant static noise called photo response non-uniformity (PRNU). It can be expressed as a percentage (according to the EMVA1288 standard) using the following formula:

$$PRNU_{1288} = \frac{\sqrt{s_{grey} - s_{dark}}}{\mu_{grey} - \mu_{dark}} [9] \tag{2.5}$$

Where μ_x stands for the mean of frame x and s_x stands for the static variance [9]. The PRNU can be compensated by multiplying each pixel with its corresponding gain value [2].

2.5.3 Dark Signal and Dark Current Non-uniformity

The dark signal is a result of the thermal generation in silicon creating EHP as a result of defects in silicon [16]. The dark signal depends on integration time and also has a strong dependency on temperature (doubling with a temperature variation of a few degrees). The dark signal non-uniformity (DSNU) is the static noise resulting from the static variance of the dark signal similar to the PRNU. It can also be expressed (in number of noise e^-) using the following formula:

$$DSNU_{1288} = \frac{s_{dark}}{K} [9] \tag{2.6}$$

Where K is the sensor gain (digital number in the image per electron) and s_{dark} is the static variance of the dark current. The DSNU can theoretically be completely corrected in post-processing as well. This requires data of the dark current for each pixel for different temperatures and integration times. Measuring the dark current can be difficult because the sensor temperature has to be kept very constant as a result of the low doubling temperature. In recent technology nodes, the dark current has reduced drastically (a factor of 10 per technology node) [24].

2.6 Image Sensor Characteristics

While the temporal and static noise are important metrics, there are other factors that define the performance of image sensors as well. In this section, the most important of these are discussed.

2.6.1 Fill factor

The fill factor (FF) is the ratio of the light sensitive area compared to the total pixel area. The non-light-sensitive part is being occupied by isolation between the pixels, transistors and sometimes capacitors. As a result, a more complex pixel architecture will often result in a lower fill factor. The FF is important because a larger photodiode can collect more photons, resulting in a larger SNR as explained in section 2.7.

2.6.2 Quantum Efficiency

The quantum efficiency (QE) defines the ratio of EHP generated per photon hitting the pixel. According to the convention used in EMVA1288 [9], the amount of photons hitting the complete pixel area has to be accounted for in the formula, not only the photons hitting the light sensitive area. The fill factor is thus included in this definition.

The QE is also wavelength dependant. A photo diode can be tuned to operate optimally for a specific wavelength by changing the doping concentration and depth of the PN depletion region [16]. Another strategy to improve the QE is to use back side illumination (BSI). In BSI sensors, the wafer is thinned and the light reaches the image sensor from the back side instead of having to travel trough all BEOL layers (figure 2.7). This will result in more photons reaching the photodiode. BSI requires exta process steps and increases the cost of an image sensor.

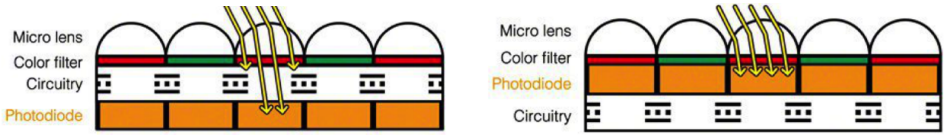

(a) Front side illumination. (b) Back side illumination.

Figure 2.7: Back VS front side illumination. Courtesy [5].

2.6.3 Charge-to-voltage Conversion Factor

An electron collected in the PD is converted to a readout voltage at the output of the sensor. The voltage difference per electron at the output is called Charge-to-Voltage Conversion factor (CVF) or sometimes called conversion gain. This depends on the FD capacitive value and on the gain of the readout circuit. A low gain will increase the contribution of the readout, while a large gain can saturate the readout electronics.

2.6.4 Full Well Capacity

After collecting a certain number of EHP's, the image sensor will saturate. This can be the result of saturation in the FD, PPD, ADC or the readout circuit. The maximal amount of EHPs the sensor can read out before saturation is called the full wel capacity (FWC). A larger FWC thus requires larger pixels. This parameter limits the upper limit of the dynamic range.

2.6.5 Linearity

Often it is desirable to have a linear dependancy between the incoming photons and the ouput of an image sensor. In that case, any deviation from this linear response

is an unwanted effect. There are multiple definitions for this non-linearity (NL). The nominal definition used at Caeleste uses the following formula:

$$NL[\%] = \frac{E_{max}}{FS} * 100[1] \tag{2.7}$$

Where E_{max} is the maximal deviation from the linear fit between 0 and 90% of the FWC, and FS is the full scale in the same unit as the maximal deviation [1]. Non-linearities can be the result of several components in an image sensor, for example the readout buffers or the capacitors to store charge. The pixels itself also contribute to the non-linearity. The conversion from photons to charge in the photodiode is almost completely linear [25].

2.6.6 Image Lag

It is possible that, especially in larger pixels, there is some residual charge left at the PPD after the charge transfer to the FD. This will cause some information to be retained from one frame to the next, resulting in ghosting artefacts in the images. There are several causes for image lag. For example a potential barrier can prevent a fraction of the charges from reaching the FD during charge transfer (shown in figure 2.8) [46]. A potential pocket in a PPD can have the same effect.

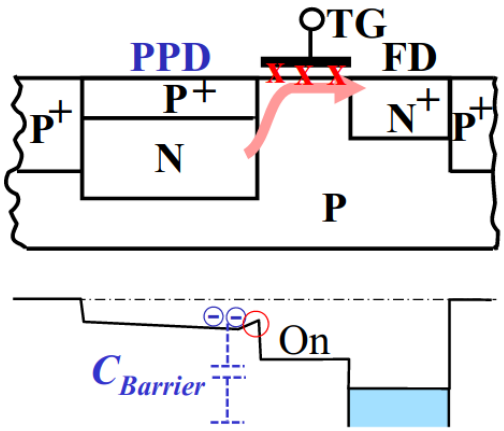

FIGURE 2.8: Image lag caused by a potential barrier in the PPD. Courtesy [46].

2.7 Signal-to-noise Ratio and Dynamic Range

The signal-to-noise ratio (SNR) of an image sensor is the ratio between the signal power to the noise power at the output of the sensor, often expressed in decibels. This is an important metric since it influences the quality of an image. Both the signal and the noise (ex. DCSN) depend on the illuminance. Therefore, the SNR is often plotted in function of illuminance or in function of the photo current.

$$SNR = 10log_{10}(\frac{P_{signal}}{P_{noise}}) \tag{2.8}$$

The dynamic range is the ratio between the lowest and highest detectable light intensity, often expressed in decibels. There exist many definitions for dynamic range, depending on what is defined as the maximum and minimum detectable signal [18]. The lowest detectable signal is generally considered to be the illuminance for which the sensor has a noise power equal to the signal power [16]. This limit is chosen higher, especially when the image is meant to be shown to a human since a SNR of zero decibels will not produce beautiful results. The highest detectable signal can have several limitations. It is possible to take the point where the input SNR becomes zero again as will be explained later in this section. Another possibility is the illuminance for which the FWC is reached [9]. Some sensors are limited by the ADC range or can have saturation in the readout circuit, and in that case, this saturation point is considered the upper limit [9]. Finally, for linear sensors, a point where the sensor is no longer linear enough is sometimes chosen as the upper limit. For this thesis, the dynamic range will be defined as the range between the point where the SNR becomes larger than zero decibels until the point where the SNR becomes lower than zero decibels again since this is the most general definition [18].

A theoretical model for the temporal noise can be found using the assumption that the noise between all the pixels is independent and all the noise contributions described in section 2.4 are independent. The result of these assumptions are that the temporal noise sources can be added up [9] [24]:

$$\sigma^2_{total,output} = \sigma^2_{ph} + \sigma^2_{dark} + \sigma^2_{reset} + \sigma^2_{reset} + \sigma^2_{other} \tag{2.9}$$

Using this formula and equation 2.1, 2.2, 2.4, the total SNR at the output of a linear sensor can be written as:

$$SNR_{output} = \frac{I^2_{ph} t^2_{int}/q^2}{I_{ph} t_{int}/q + I_{dark} t_{int}/q + kTC/q^2 + C^2_{fd}\overline{v^2_{readout}}/q^2 + \sigma^2_{other}} \tag{2.10}$$

$$= \frac{I^2_{ph} t^2_{int}}{q(I_{ph} + I_{dark})t_{int} + kTC + C^2_{fd}\overline{v^2_{readout}} + q^2\sigma^2_{flicker} + q^2\sigma^2_{other}} \text{[26]} \tag{2.11}$$

The static noise can be considered as part of the total noise as well [18]. This noise can be corrected completely in theory. So if it is included in the definition of dynamic range, the dynamic range will depend on the performance of the correction algorithm.

As can be seen in figure 2.9, The SNR has two different slopes of 20dB/decade for low light intensities. and 10dB/decade for high light intensities. This is because at low illumination, the photon shot noise is less important and as a result the SNR will increase in a squared relation to the photon current. For high intensities however, the SNR is photon shot noise limited. This limitation cannot be overcome since it is a physical property of the light itself.

The expression for SNR in equation 2.11 is only valid for linear image sensors.

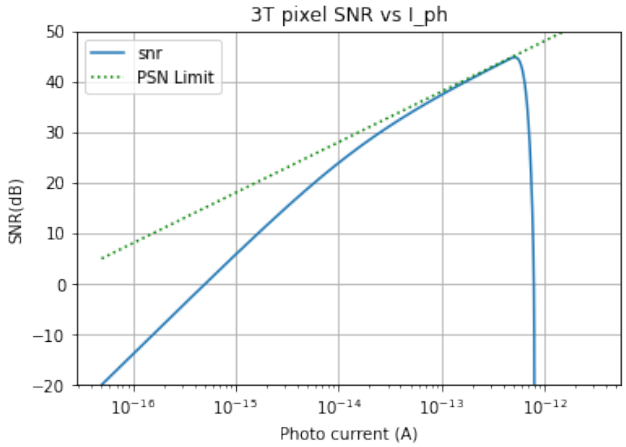

FIGURE 2.9: SNR curve of a typical linear sensor with a non-linear saturation and the PSN limit.

The SNR curve for a non-linear sensor can be calculated analogue to the method described in the previous section [26]. This is however an expression for the SNR at the output signal. Most of the time the actual illuminance of each pixel is required. In that case, when the slope of the photoresponse curve becomes small, a small error on the output signal will correspond to a large error on the input signal [8]. It is therefore useful to define the input SNR as well, which can be calculated as:

$$SNR_{input} = \frac{\mu_p}{\mu_y} \left| \frac{\sigma\mu_p}{\sigma\mu_y} \right| SNR_y[8] \tag{2.12}$$

In case of a perfectly linear sensor, The input SNR will be exactly the same as the output SNR before saturation and become zero after saturation. Most image sensors however have a smooth transition between the linear region and saturation region, resulting in a decreasing SNR slope near saturation as shown in figure 2.9.

As will be explained in the next chapter, there exist several methods to increase the dynamic range. When comparing these techniques, the SNR will thus be an important metric to compare the SNR of the different sensors. Some of the HDR sensors modify the shape of the photoresponse (ex. logarithmic response or linlog shape) [16] [24]. For this reason, it is important to use the input SNR instead of the output SNR to measure the performance of an image sensor.

Chapter 3

HDR Image Sensors

A standard linear image sensor can not always achieve the required dynamic range. This chapter will discuss different methods that increase the dynamic range and the trade-offs of all these methods. First, an overview of HDR imaging methods is given. Afterwards, all these methods will be investigated in more detail.

3.1 HDR Methods

The most known method to increase the dynamic range is capturing multiple images, each with a different integration time, and combining them in software [37]. The images with a longer integration time will contain less noise at low illumination, and the images with a shorter integration time will be able to capture scenes under high illumination without saturating. No special hardware is required for this method and it is therefore popular in consumer cameras. The problem with this approach is that, when the scene contains moving objects, this will result in ghosting artefacts in the final image. For this reason, true HDR pixels have been developed that require only one integration period, and thus do not suffer from these artefacts.

One method to create a true HDR image sensor is by modifying the shape of the response curve. For example using a logarithmic response curve, lin-log curve or S-curve sensors has been proposed [26] [16] [6]. Another method is to use multilinear pixels which approximates the logarithmic response by a series of linear responses [26].

It is also possible to keep using a linear sensor, but do multiple non-destructive readouts after each integration period, all with another gain [24]. The high gain frame will then contain less noise and the low gain frame will have a higher saturation level. This is similar to varying the integration time, but with only one integration period. These pixels do require some extra hardware to do this. The frames then have to be combined using software methods similar to the frames obtained by changing the integration time.

Finally, there have been some new methods proposed recently that operate dif-

ferent from classical image sensors, often by adding more logic to each pixel. The information in in these pixels is no longer only read out by converting the photocurrent to a voltage at the output of the sensor, but can be recovered from other effects. It is possible to achieve a very high dynamic range in these sensors.

3.2 Logarithmic Image Sensors

To have the optimal dynamic range, a steeper slope in the photoresponse curve at low illumination is required to increase sensitivity there, and thus make the lowest detectable limit smaller [18]. A flatter slope at higher intensities is required to increase the saturation level and thus increase the highest detectable limit. A logarithmic image sensor has this effect. A simple implementation to create such a behaviour can be realized by connecting the gate of the reset transistor to the drain of that transistor [16]. A schematic of such a logarithmic pixel is shown in figure 3.1. This pixel does not have an integration period and readout period, but the photocurrent is continuously converted to a voltage at the FD. The SNR can be modelled as:

$$SNR(I_{ph)}) = \frac{I_{ph}^2}{(I_{ph} + i_{dc})^2 const} [26] \tag{3.1}$$

Where the constant factor depends on the readout noise, FD capacitance and the parameters of the reset transistor. As can be seen in this formula, the SNR is almost independent of the photocurrent i_{ph} when the photocurrent is much larger than the dark current. This formula is however for the output SNR. Because of the flat photoresponse slope at high illuminations, the sensitivity and thus the input SNR will decrease for high illumination (section 2.12).

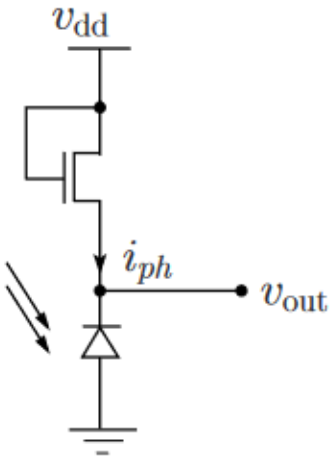

Figure 3.1: Schematic of a logarithmic image sensor. Courtesy [26].

These pixels suffer from high FPN as a result of process variations in the reset transistor [26]. CDS is also no longer possible since this requires a linear response, even further increasing the FPN and decreasing the SNR [26]. The pixels also show a temperature dependency [16]. The non-integrating nature of these pixels increases the noise compared to integrating pixels [26]. The readout circuit is also challenging to design as a result of the limited voltage swing at the output of the pixels [32].

3.3 Multilinear Image Sensors

Instead of using a true logarithmic response, the idea here is to use a piecewise linear response to approximate a logarithmic response [26]. Contrary to the logarithmic pixel, multilinear pixels are integrating pixels, resulting in a higher SNR [16]. An example of such a response for four segments can be seen in figure 3.2. The amount of segments can vary depending on the implementation. This behaviour can for example be created in a 3T pixel by controlling the voltage at the reset gate and thus the full well capacity. First, the FWC is kept low by applying an intermediate voltage on the reset transistor, causing overflow when the voltage on the FD becomes too low [24]. After a certain integration time, the FWC is increased by turning off the reset transistor completely. This will create a multilinear response curve where the characteristics can be controlled by changing the reset voltages and the integration time between the steps. The collected charge in function of time can be seen in figure 3.3 for different light intensities. It is possible to extend this method to 4T pixels as well by manipulating the TG voltage [17]. The equation for the SNR is:

$$SNR(I_{pj}) = \begin{cases} \frac{(I_{ph}t_{int})^2}{q(I_{ph}+I_{dc})t_{int}+\sigma_{readout}} : 0 < I_{ph}t_{int} < Q_{sat\theta} \\ \frac{(I_{ph}(t_{int}-t_1))^2}{q(I_{ph}+I_{dc})(t_{int}-t1)+\sigma_{readout}} : Q_{sat\theta} < I_{ph}t_{int} < Q_{sat} \end{cases} \quad [26] \qquad (3.2)$$

As can be derived from this equation, an SNR dipp will occur at the boundary between the segments. A trade-off will have to be made between the SNR dip and dynamic range improvement, and more segments will result in a smaller dip. CDS could be done on multilinear sensors, but is only effective at low illumination before the first knee-point [26]. The DAC that controls the reset voltages has to drive a large parasitic capacitance, and because of this, these pixels have not been popular until recently [16].

3.4 Multiple Capture Image Sensors

This technique relies on the non-destructive readout of multiple frames, each with different gains. There are several methods to create these different gains. A method to combine the frames into an HDR image is discussed in section 5, where the information of the higher gains is used for the low illumination part of the sensor. The information of the low gain frame is used for the high illumination parts, where the high gains are saturated. The larger the difference between the gains, the higher the dynamic range improvement. But at the point where one of the gains saturate,

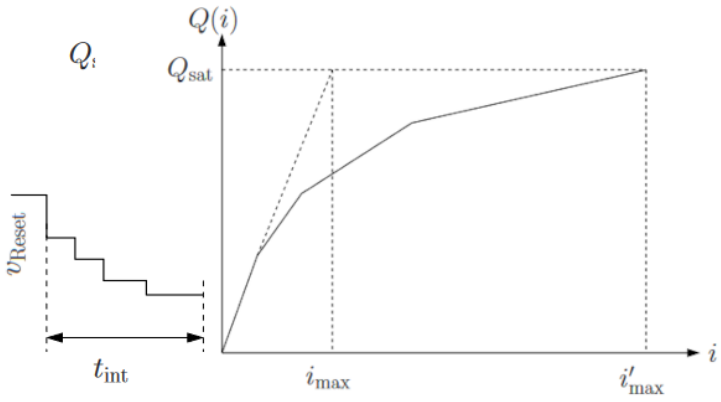

FIGURE 3.2: Multilinear response curve. Courtesy [26].

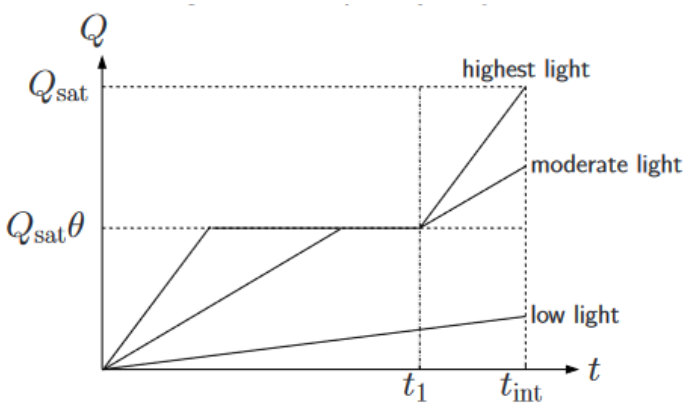

FIGURE 3.3: Multilinear sensor charge in function of time. Courtesy [26].

there will be an SNR dip, and the larger the difference between the gains, the larger this SNR dipp will be. This is a trade-off when selecting the proportions between the different gains in such a sensor, similar to multilinear pixels.

There are several methods to implement this. It is for example possible to create a variable FWC in a basic 4T pixel by adding an extra capacitor that can be connected to the FD by a merge switch (figure 6.1) [28]. The high gain is read out first, afterwards, the merge switch is turned on, and the low gain is read out. The charge that initially does not fit on the FD capacitance has to overflow to the extra low gain capacitor. Figure 3.4 shows two methods to achieve this, either by overflowing the charge over the TG (DC overflow method) or overflowing over the TG (three level TG method) [28]. Another pixel architecture is shown in figure 3.6a. In this pixel, the low gain is read out first, and afterwards the high gain can be read out by pushing the charge back to the FD by turning off the mos capacitors [28]. It is

also possible to split the diode into a large and small part [51] as shown in figure 3.6. These can then both be read out after each other. An array of different pixels can also be created, where some pixels have a higher gain than others [26]. For example by giving some pixels a higher integration time or different FD capacitance. The dynamic range will be increased at the cost of resolution.

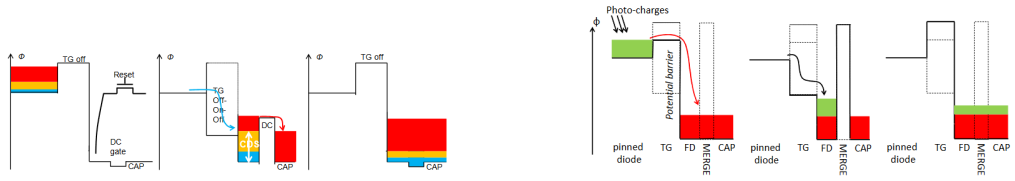

(A) DC overflow method (B) 3 level TG method

FIGURE 3.4: Multiple capture pixels. Courtesy [28].

Equation 2.12 shows how the formula for the SNR in function of the photocurrent. In this equation, it is possible to create a difference in gain for a certain illumination by changing the integration time, FWC or the photocurrent (split diode pixel). Figure 3.5 shows the SNR curve when making the FWC five times smaller, and when making the integration time five times larger for a certain photocurrent. Increasing the integration time just results in a shift of the SNR curve to the left region (when dark current shot noise can be ignored).

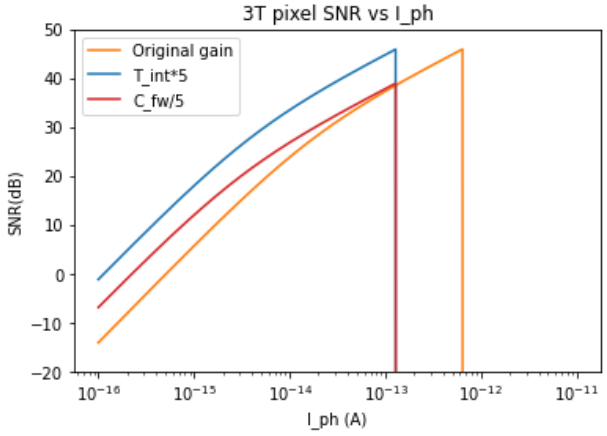

FIGURE 3.5: Comparison of multiple capture techniques.

The downside of these image sensors is that all the samples have to be read out individually, resulting in a lower frame rate compared to the logarithmic and multilinear sensors. Another downside is the reduced fill factor because of the extra hardware that is required for this sensor. CDS is still possible in this method because of the

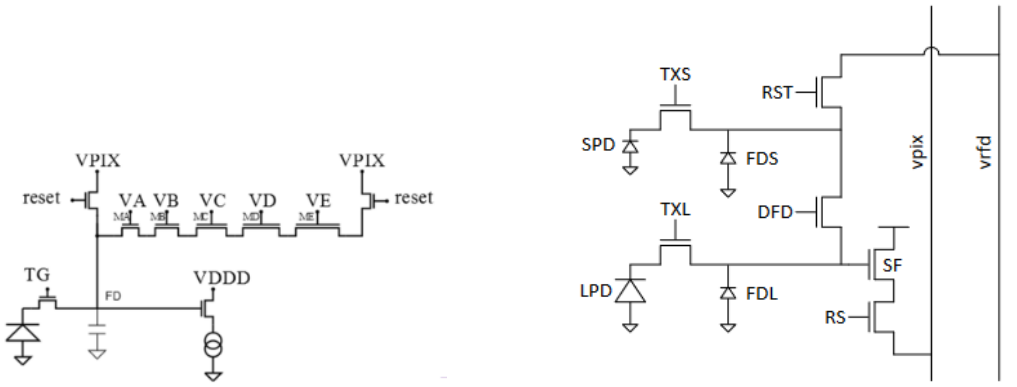

(A) Pushback HDR pixel. Courtesy [51]. (B) 3 level TG method. Courtesy [28].

FIGURE 3.6: HDR pixels.

linear nature. These pixels will thus have lower spatial and temporal noise compared to the previous methods.

3.5 Other Methods

Instead of converting the light intensity to a voltage, and then recovering the illuminance from this voltage, some pixels that acquire the information in some other manner have recently been published. An example is a time to saturation pixel, where the integration time needed before a pixel becomes saturated carries the information. These pixels directly output a digital number [16].

Light to frequency pixels or spiking image sensors operate similar to the human eye. The photocurrent is converted to a pulse train with a frequency depending on the incoming light [11]. This is an asynchronous pixel, meaning that the readout is frameless, and the spikes occur in real-time. It is not straightforward to reconstruct an image suitable for visualization from this information, but this data could be used directly in machine vision applications.

Self reset pixels operate the same as normal pixels, but automatically reset when the the pixel becomes saturated [41]. This means that if there are M resets, the dynamic range will be increased $20log(M)dB$. The amount of resets that occurred during the total integration period will form the most significant bits of the data, and the charge left at the end of the total integration period will form the least significant bits.

The disadvantage of all these pixels is that they require a lot of transistors, resulting in a low fill factor. These pixel types may become more popular in the future, when smaller technology nodes are available, since the relative area of the transistors will decrease for a certain photodiode size. The pixels can all achieve a very high dynamic range.

3.6 Conclusion

An overview of HDR image sensor implementations is given in this chapter. Modifying the photo response will increase the dynamic range with very little extra hardware per pixel, but this implementation suffers from high FPN and cannot do CDS effectively. Multiple capture image sensors operate linearly and thus can still do CDS, but require extra transistors and extra readouts, lowering the speed of the sensor. Finally, there have been some other pixels proposed recently that increase the dynamic range by doing in-pixel processing, at the cost of an even lower fill factor.

Chapter 4

Non-uniformity Correction

There are several static noise sources that can, in theory, be corrected completely as explained in chapter 1. This correction is not only needed to create good-looking images, but is also required when merging the HDR images produced by some HDR image sensors. The static noise and non-linearity can also interfere with some characterization measurements, for example a quantum efficiency measurement. This chapter will discuss a theoretical model for a calibration based image correction. The goal of the non-uniformity correction is to compensate for this static noise and non-linearity in the digital domain. This correction algorithm has to be generic enough to be compatible with most existing and future Caeleste image sensors while still using the sensor specific knowledge for an optimal performance. The amount of calibrations to be performed for each sensor is best kept to a minimum. All the theoretical methods proposed in this chapter will be tested on real sensors later. The correction method should also be drift resistant in order to avoid that calibrations are needed every time the sensor is used under different operating conditions, since these calibrations can only be done in a lab environment and can be time-consuming. Some image sensors do CDS on chip and some sensors output both the reset and the signal frame. The correction can be different for both cases. The proposed correction method is optimized for CISs that have CDS implemented.

4.0.1 Literature Review

There are two options to correct an image: calibration based image correction and scene based image correction [12]. The scene based correction estimates the correction parameters in real time based on the scene, sometimes relying on artificial intelligence [47] [48]. This can be unpredictable and for this reason, a calibration based image correction method is implemented in this thesis. The most used non-uniformity correction is the 2 point logarithm [12] [40] [29]. This algorithm assumes that the pixel response for each pixel is linear:

$$V_{out,i} = a_i L_{in,i} + b_i [12] \tag{4.1}$$

Where L_{in} is the illuminance at the i^{th} pixel and $V_{out,i}$ is the output voltage for the i^{th} pixel. These pixels can have a different gain a_i and different offset b_i. Thus, two

measurements are required: a dark image to find b_i and a gray image to find a_i. This method does not correct the non-linearity. To correct this as well, one possibility is to use a multiple-point linear interpolation instead of the two-point method [12]. Recently, interpolation using polynomials or splines has been used as well [43] [33]. Another possibility to correct the non-uniformity is a lookup table based approach. [21]. A polynomial approximation based approach has been implemented because it can correct static noise and the non-linearity while it only has to store a few parameters per pixel.

Variations in operating conditions can reduce the effectiveness of the correction. The dark current and the corresponding DCNU is the most sensitive to these variations and thus has to be estimated when there is a change in the operating conditions. The simplest method is to take a reference dark frame where a mechanical shutter blocks the light, and subtract this from the actual image. But this shutter is often no longer used in CIS. Some sensors have implemented a large amount of temperature sensors between the pixels to estimate the dark current [10]. Section 4.3 will describe a method to estimate this dark current per pixel, suitable for most Caeleste sensors.

4.1 Order of Corrections

In an image sensor, the received light intensity L_{in} in each pixel is converted to a voltage at the output of the sensor, ideally linearly dependent to the incoming light. There are a number of non-idealities that cause the output voltage to differ from the input voltage. The output voltage can be modelled by a non-linear function of the received light intensity $f(L_{in})$, different for each pixel, and depending on the operating conditions. The correction algorithm has to apply the inverse of $f(L_{in})$ to the sensor's output to determine the light intensity at the pixel. In figure 4.2, the sources of these non-idealities in an image sensor are plotted at their location in a generic CMOS pixel. These errors have to be corrected in the inverse order in which they occur [19].

Figure 4.1: Basic concept of image correction.

The first error introduced in the sensor is the dark current and the corresponding DCNU. These are introduced at the photodiode and storage node. The dark current is introduced before any non-linearities of the readout chain and therefore has to be corrected after all the other corrections.

The next error introduced is the photoresponse non-uniformity and non-linearity. The PRNU is mainly the result of process variations in the SN capacitance and source follower. The non-linearity is introduced everywhere in the sensor, mainly caused by the source follower and a non-linear SN capacitor [2]. Since it is introduced per pixel, not all the pixels will have the same non-linearity.

The readout chain also introduces offsets and non-linearities. Since the main source of the non-linearity is introduced in the pixel, the non-linearities introduced in the readout chain are not corrected separately and only the offsets of the readout amplifiers are taken into account.

The complete order of operations is thus: correct the offset introduced in the readout chain for each column, then correct the PRNU and non-linearity of each pixel, and finally subtract the dark current. These calibrations require a photoresponse and dark current measurement of the sensor in a lab environment.

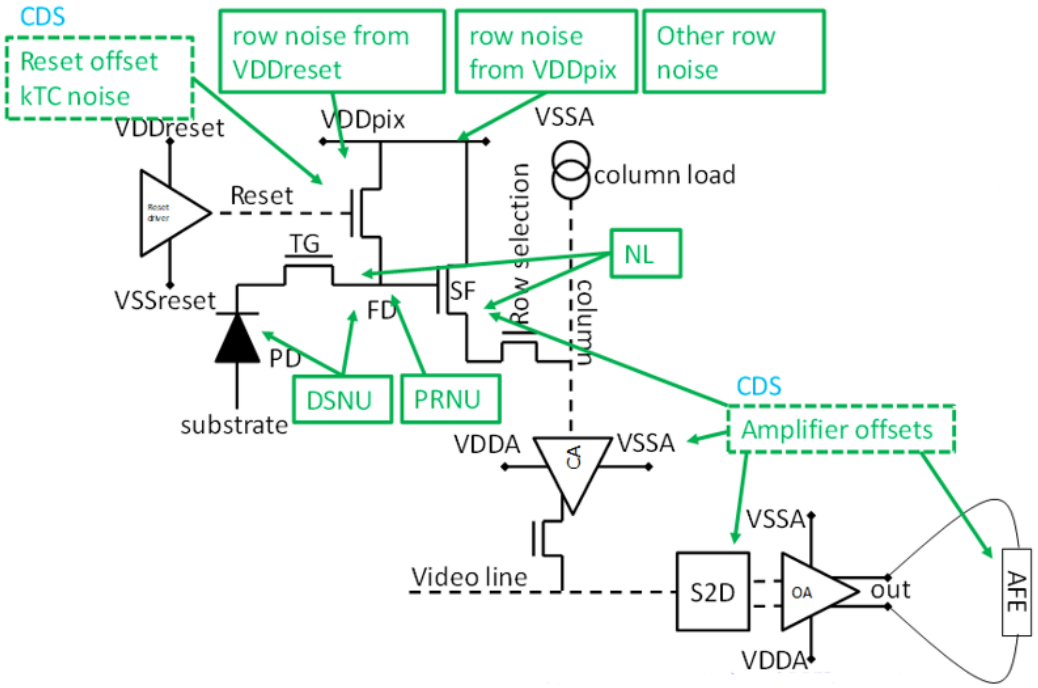

FIGURE 4.2: Non-idealities and their order of occurrence in an image sensor. Courtesy [2].

4.2 Defect Pixels

It is important that the defect pixels are not included in the calculation of mean values during calibration. A defect pixel can be a lot of things: for example a pixel can be insensitive to light, can have a dark current that is too large compared to the other pixels or can have a deviating photoresponse. It is also possible that an entire column or a cluster of pixels is defect. These defects are not only caused by defects in the silicon but can be caused by contamination of the lens as well. Caeleste has developed a software framework to test for bad pixels and map them [3]. The first step of the correction will be to run this algorithm and exclude these bad pixels from here on. The value of these pixels can be reconstructed by a post-processing algorithm, so the sensor is still usable when there are some defect pixels present. This reconstruction is not part of this thesis. It is also important to exclude the test rows that are used for characterization, present in most image sensors.

4.3 Dark Current Correction

The dark current is the first noise source introduced in a pixel, and thus should be compensated for last. It is discussed first because the dark current is needed to find the other required calibration data. The dark current can be modelled as a non-linear function dependent on both the temperature and the integration time, and different for each pixel. A method proposed at Caeleste was to do a linear approximation of this dark current and scale it using the mean of the dark pixels. This can be modelled as:

$$I_{dark}(T,t,i) = i_{dark,i} * \frac{I_{dark,mean}(T,t)}{i_{dark,mean}} \tag{4.2}$$

Where $I_{dark}(T,t,i)$ is the dark current of the i^{th} pixel in function of the temperature T and integration time t. $i_{dark,i}$ is the dark current of pixel i at the moment of calibration. This dark current is then scaled by the scaling factor: $\frac{I_{dark,mean}(T,t)}{i_{dark,mean}}$. This factor is the ratio of the mean dark current of the whole sensor to the mean dark current during calibration. This has been verified and is shown on figure 4.3a where the dark current for some random pixels is plotted in function of the mean dark current. The relationship is indeed linear for all the pixels.

In the case of off-chip CDS, it is easy to find the dark current for each pixel: The difference between the signal and reset frame in the dark will only contain the dark current. For on-chip CDS, this is more difficult. The dark image after CDS contains both the dark current and readout offsets, and it is not possible to differentiate the dark current from these offsets. The separation of the two offsets is needed since row offsets have a far smaller temperature and integration time dependency than the dark current. The solution for this is to take one image with a long and one image with a short integration time. The difference of these images divided by the difference in integration time results in the dark image [1].

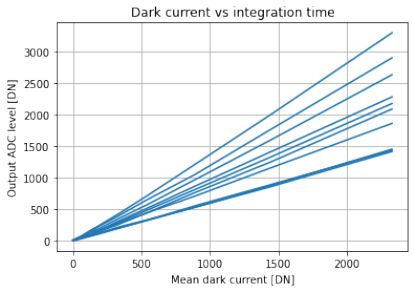

(A) Dark current of random pixels VS mean dark current. The dark current is measured by changing the integration time, showing a higher dark current for longer integration times.

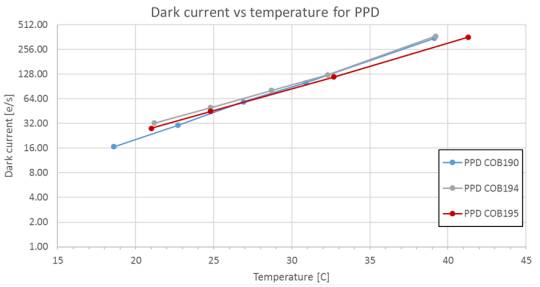

(B) Dark current for a varying integration time for different COBs. Courtesy [13].

FIGURE 4.3: Dark current.

This approach cannot compensate the dark current completely. The relation between the temperature and the dark current is exponential [49]. Thus, when scaling the dark current of each pixel to the average dark current, this method will only do a linear interpolation of this exponential function. The dark current is not completely linear dependent on the integration time as well, but this effect is small [50]. A temperature gradient on the chip will also introduce an error when using this method, as can be seen in figure 4.4. The temperature gradient in this case is the result of the south side of the chip heating up more due to the presence of most of the back end there (column buffers, output buffers, ...). The dark current on the hot side is more than double the dark current on the cold side. This error cannot be corrected since the temperature at each position often cannot be measured in real time, only a global scaling factor is used. Finally, there are multiple sources of dark current: at the PPD and all the storage nodes. In the current implementation, this separation is not taken into account. This introduces errors as well. For example, when the integration time in a global shutter image sensor is changed, the time that the charge has to be stored on the storage node does not change, only the PPD dark current will thus increase. A measurement of all the sources separately is difficult, as it requires writing a new timing scheme for each sensor. Estimating the mean dark current of all the sources in real time is also more difficult. This is not implemented for these reasons. Often, one of the two contributions will be dominant, and the error made is small [13][45].

The next required step is to estimate the scaling factor. The best solution is to try to estimate it using the black pixels that are often included for characterization purposes. The only type of black pixels suitable for this are EB0 pixels (pixels with optical shielding of the photodiode). Other types of black pixels such as EB4 (extra TG always on to flush the pixel permanently) will not have any PPD dark current. These could be used however for the estimation of the dark current in global shutter

since the FD dark current will often be dominant in that case. Also, it would be better to place the black pixels perpendicular to the temperature gradient instead of parallel as is now often done. In that case, It would be possible to estimate the temperature gradient in real time as well. Enough of these pixels are needed to get a good estimation of the average dark current. When there are no black pixels available, It could still be possible to estimate the dark current by using the integration time and a build in temperature sensor that is often available. If the latter is also not possible because of the lack of a temperature sensor, the only option would be to re-calibrate the sensor again by taking a new dark image when the temperature changes. It has been proposed to estimate the temperature by using "hot pixels" [23]. These pixels have a very high dark current because of defects. The last method has not been implemented.

Because of all these errors, the calibration of the dark current will work best if the sensor is working in the same operating conditions as when the calibration was done and the performance will deteriorate the further the operation conditions are removed from the calibration point. It is therefore advised to do the dark current measurement under nominal operating conditions and wait until the temperature of the sensor is settled, instead of doing the dark current calibration immediately after the start up of the sensor.

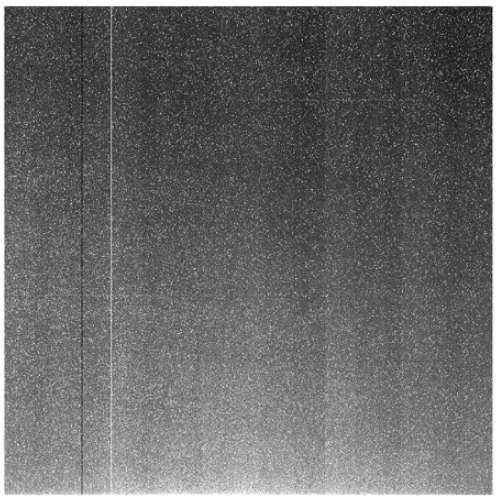

Figure 4.4: Temperature gradient in a dark current image.

4.4 Readout Offset

When CDS is done on-chip, there are still some offsets introduced after the CDS operation as a result from the offset from amplifiers, buffers, ... in the analog circuits. An example of this is shown in figure 2.6 where it is clearly visible which ADC

sampled which columns. Since the readout path is the same for all the pixels in the same column, all these in a column will thus have the same offset. It is thus not necessary to store the offset per pixel, but only one value has to be subtracted for each pixel in the same column.

However, This is not always the case: For example on some sensors, an inter-

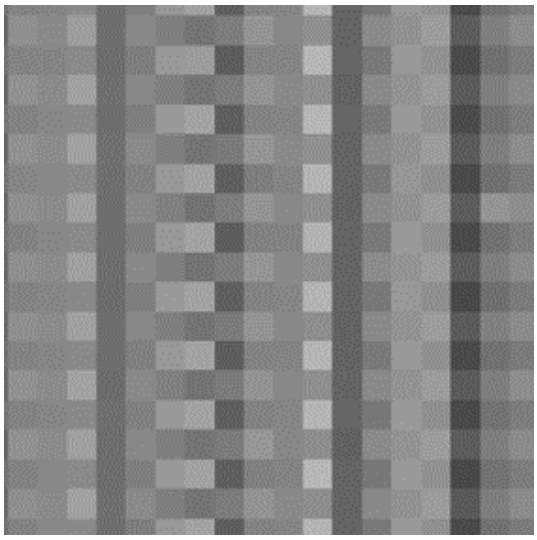

FIGURE 4.5: Zoomed in section of the readout offset.

leaving mode is used to increase the speed of the readout (figure 4.6), resulting in different readout paths in the same column. This is visible in the dark image as well. Figure 4.5 is a zoomed in section of the dark image. In this figure, it is clearly visible that there are two separate readout paths for each column. The solution is thus to store not one offset value for each column but one offset value for each readout path in each column.

To calculate these offset values, an image has to be taken in the dark. Preferably, the average is taken over several dark images to eliminate temporal noise. Then the dark current has to be subtracted from this frame and the mean of each column or readout path is taken (bad pixels not included).

4.5 Photoresponse Non-uniformity and Non-linearity Correction

After the readout offset has been corrected, the photoresponse non-uniformity and, when the sensor is not completely linear, a non-linearity correction are done. These corrections can be done by approximating the photoresponse curve of each pixel:

$$V_{out,i} = f_i(L_{in}) = a_i\phi(L_{in}, 0) + b_i\phi(L_{in}, 1) + c_i\phi(L_{in}, 2) + ... \tag{4.3}$$

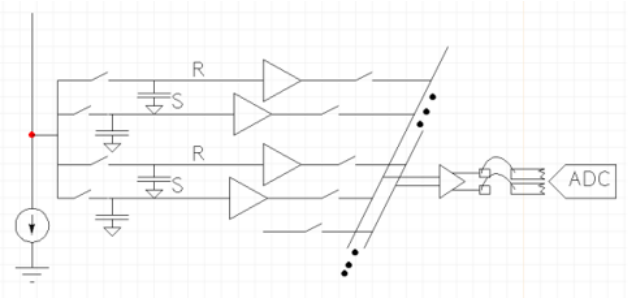

Figure 4.6: Interleaved readout chain. Courtesy [34].

Where $\phi(x, i)$ are the basis functions, preferable the monomial basis: $\phi(L_{in}, p) = L_{in}^p$, because the low complexity. L_{in} is the incident light power and $V_{out,i}$ is the output voltage for the i^{th} pixel. The advantage of this approach over an interpolation based method is that only the factors $a_i, b_i, c_i, ...$ have to be stored per pixel instead of all the interpolation points. The problem is that not L_{in} but $V_{out,i}$ is known at the output of the sensor. When using the monomial basis, the required order for a good fit can also become large because of the shape of the photoresponse. The solution is to do the inverse: approximate the input light intensity by the measured output voltage, using powers of the measured output voltage as basis functions:

$$L_{total,i} = a_i(f_i(L_{in}) - r_i) + b_i(f_i(L_{in}) - r_i)^2 + ... = L_{in} + L_{dark,i} \tag{4.4}$$

In this equation, r_i is the readout offset of the i^{th} pixel, a_i is the PRNU correction factor and b_i is the second order non-linearity correction term (it is also possible to use a higher order). It should be noted that L_{total} contains both the incident light intensity and the signal resulting from the dark current. No constant term is needed in this expression, since the readout offset correction corrects all the offsets except for the dark current after CDS.

To calculate all the factors in the equation above, a photoresponse measurement is required. This is done by placing a controllable light source in front of the image sensor without using a lens to create a uniform illumination over the whole sensor [1]. Then the light source intensity has to increase in a number of steps (around 50-100 steps is advised) and a frame has to be captured at each step. It is better to capture multiple frames at each illumination step to reduce the temporal noise. It is very important that the illumination is uniform or incorrect correction factors will be calculated, resulting in an error when the sensor is used in practice. The absolute light level is also needed for this correction. For this purpose, a reference photodiode is used to measure the illumination at each step of the light source. [1].

Using the measured photoresponse, it is now possible to calculate the PRNU and NL correction factor. First, the column offset and dark current have to be found using the method explained in section 4.3 and section 4.4. For each pixel, the factors

can be found by solving equation 4.4 using the least squares method:

$$\begin{bmatrix} L_{in,0} \\ L_{in,1} \\ \vdots \\ L_{in,n} \end{bmatrix} + \begin{bmatrix} L_{dark,i} \\ L_{dark,i} \\ \vdots \\ L_{dark,i} \end{bmatrix} = \begin{bmatrix} (f_i(L_{in,0}) - r_i) & (f_i(L_{in,0}) - r_i)^2 \\ (f_i(L_{in,1}) - r_i) & (f_i(L_{in,1}) - r_i)^2 \\ \vdots & \vdots \\ (f_i(L_{in,n}) - r_i) & (f_i(L_{in,n}) - r_i)^2 \end{bmatrix} \begin{bmatrix} a_i \\ b_i \end{bmatrix} \tag{4.5}$$

Where, $L_{in,x}$ is the illuminance measured by the reference photodiode at step x in the photoresponse measurement. This least squares equation has to be solved for all the pixels individually. The least square will minimize the squares of the residuals. For this, it is necessary to define the saturation point until where the residuals have to be minimized. Choosing this point too low will lead to a reduced dynamic range. Choosing the point too far will lead to a larger error after correction, because the least squares will try to fit to the saturated part as well. To solve this, a weight function is used that is proportional to the derivative of the photoresponse. As a result, the flatter the photoresponse curve becomes, the lower the weights will become resulting in a good trade-off between dynamic range and correction errors after correction. Also, an absolute error at low illuminance results in an increased relative error because the signal power is low. Therefore, the used weight function should encourage a better approximation in the low illumination region. The following formula is used for the calculation of the weights:

$$w(L_{in}) = \frac{F'(L_{in})}{a + F(L_{in})} \tag{4.6}$$

In this case, $F(L_{in})$ is the average photoresponse over all the pixels since calculating different weights for each pixel is not worth it. The term a is used to control the shape of the weight function and this value is set to the maximal value of $F(L_{in})$. An example of a weight function is plotted in figure 4.7.

This method assumes the readout circuit is completely linear. This is not always the case. A small non-linearity in the readout chain will only introduce a ignorable error. If a second order correction is not enough, it is possible to increase the order for a better correction. This will slow down the algorithm and requires more coefficients to be stored per pixel. A second order correction will often be sufficient as will be shown in chapter 6 and chapter 7.

4.6 Off-Chip CDS Correction

All the previous methods in this chapter assumed CDS is done on-chip and thus are not valid without CDS. When the CDS is done off-chip, there are two options: either subtract the reset frame in the beginning and then proceed in the same manner as on-chip CDS, or correct both the reset frame and the signal frame individually and subtract them after the corrections. The last method is the most accurate, since CDS corrects for errors that are introduced at pixel level. The non-linearity of the

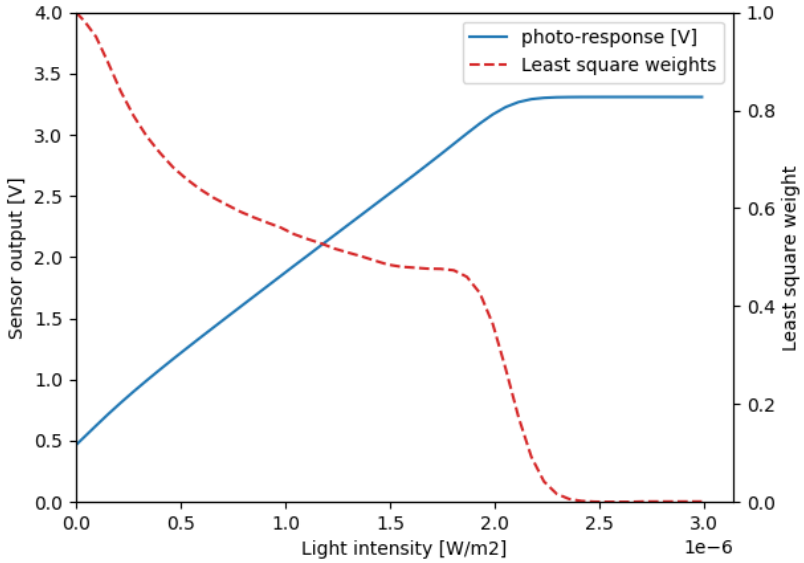

Figure 4.7: Graph showing an example of a photoresponse and the weights used for the least squares equations.

rest of the sensor will introduce an error when the reset frame subtraction is done before any corrections. This error is however small in a linear sensor and correcting both frames would require far more operations and extra calibration data as well. For this reason, the reset frame is subtracted before the correction. This has the added benefit that there is no readout offset correction needed, since this is now automatically done in the reset frame subtraction.

4.7 Performance Considerations

Speed is an important factor in the correction of images. Sometimes, a stream of images has to be corrected, and it is preferred that this can be done fast or even in real time. The method as implemented now is using floating point arithmetic and is quite slow at the moment. However, several changes can be made to improve the performance. Some possible improvements will be discussed next. This is not the focus of this thesis and these improvements will not be implemented. All the operations for the correction are linear, using only multiplications or additions, so a good speed can be achieved. Since for each pixel, some data has to be loaded (column offset, PRNU, ...), the program will probably be memory constrained.

Firstly, all the floating point operation can be converted to fixed point operations with only a small rounding error introduced. The word length of most image sensors is in the range of fourteen to sixteen bits. When carefully considering the word length at each step of the algorithm, it can be kept to a minimum. The limited word

length also means that less memory will be used and this would make an FPGA implementation possible.

Another improvement would be to parallelize the algorithm. There a lot of pixels that have to be processed and these can all be corrected in parallel. It would also be possible to use the SIMD instructions often included in a CPU. Another possible improvement would be to move the time critical operations to another programming language (for example c++) since Python is slow compared to these languages. However, it is still important to have a Python interface to work alongside the other internal software. Care should be taken to reuse the calibration settings as much as possible to prevent reloading these parameters too often.

4.8 Conclusion

In this chapter, a theoretical implementation for image correction suitable for Caeleste sensors is proposed. The proposed method is also able to remain accurate under small temperature and integration time fluctuations. This algorithm requires a photoresponse measurement and a dark current measurement. The algorithm has been implemented in Python and is slow at the moment, requiring several seconds to correct one image. The performance could be increased by implementing some improvements. The practical performance of this algorithm will be discussed in chapter 6 and chapter 7 for two different CISs.

Chapter 5

High Dynamic Range Image Synthesis

Some HDR sensors produce multiple images with different gains that have to be combined into one image. The goal is to maximize the SNR in the final image while avoiding artefacts in the transition regions between the gains. The HDR merging logarithm in this chapter is optimized for true HDR sensors, so ghosting artefacts as a result of moving objects will not be considered. First, a literature study of the existing algorithms will be done. Next, an algorithm to merge the frames and achieve the maximal SNR will be proposed, and finally, artefacts in the transition region will be considered.

5.0.1 Literature Review

Suppose there is an HDR image sensor that produces n frames with a different gain that have to be combined into a final image. After the image correction explained in chapter 4, the digital numbers at the output of the sensor are transformed to the light intensities at the input of the pixel. These still contain noise, both temporal noise, and static noise that has not been corrected. The frames can then be combined to find the HDR image using the following formula:

$$L_{out,hdr,i} = \sum_{j=1}^{n} w_j(L_{in,i,j}) L_{out,i,j} \text{ and: } \sum_{j=1}^{n} w_j(L_{in,i,j}) = 1 \tag{5.1}$$

Where $L_{out,i,j}$ is the pixel's illuminance estimation found by correcting the output of the i^{th} pixel and the j^{th} frame, and $L_{in,i,j}$ is the actual illuminance of that pixel. The challenge now is to determine the optimal weight function $w(L_{in,i,j})$. A simple solution for this is using binary weights that select the frame with the highest gain that is not saturated [35] [22]. This produces an abrupt transition region and creates artefacts in the transition region. This can be solved by using a smoother transition, for example by using a linear weight function [20]. All the frames that are not saturated contain information about the true illuminance of the pixel, and thus the noise can be averaged out by using the correct weights [27] [22] [39]. The methods

in literature try to estimate this optimal weight function by using a camera noise model. They focus on HDR sensors that achieve extra dynamic range by changing the integration time most of the time.

After HDR merging, tone mapping is needed to produce an image that looks good when displayed on a monitor. Recently, HDR fusion methods that do the combination of the HDR merging and tone mapping at the same time became popular [38]. These methods do not create the intermediate exposure map. An exposure map is sometimes useful, for example machine vision [22]. For this reason, these methods are not considered this thesis.

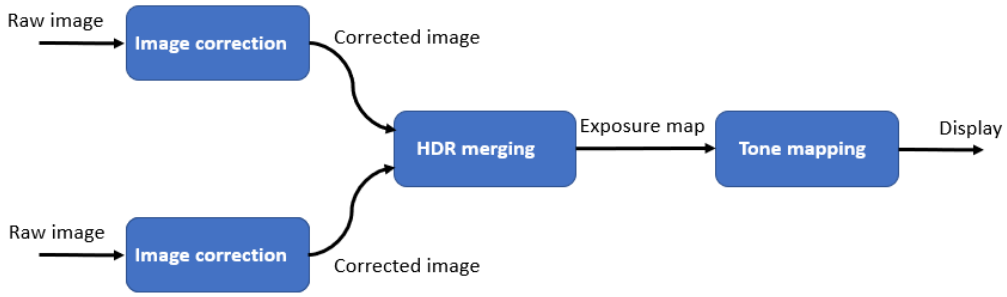

Figure 5.1: HDR synthesis software flow.

5.1 Weights for Optimal SNR

As explained by [27], it is possible to find the weights that maximize the SNR over the complete dynamic range of the sensor. But instead of trying to model the noise and then estimating the weights based on this model as is done in literature, it is possible to find the weights directly from the same photo-response measurement that was required for the image correction. Multiple frames were taken at each illumination level, and the noise can be calculated directly from these frames. When combining the frames from an HDR sensor as expressed in 5.1, the total SNR under uniform illumination can be found as:

$$SNR_{total}(L_{in})^{-1} = \sum_{j=0}^{n} w_j^2(L_{in}) SNR_j(L_{in})^{-1} \tag{5.2}$$

The derivation of this equation can be found in appendix A. Note that $SNR_j(L_{in})$ should be the input SNR instead of the output SNR (section 2.7). The weights that optimize this equation can then be found by brute forcing all the possible combinations for each value of L_{in}. This is the theoretical maximal achievable SNR possible in a certain image sensor. An example of the optimal weights for a theoretical model of a multiple capture image sensor with two gains is plotted in figure 5.2 (data generated as in section 3.4). The noise reduction is more prominent in

the region where the SNR curves of the multiple gains have a value close to each other.

These weights are a function of the illuminance L_{in} at each pixel. The actual illuminance is not known, but instead, only an estimate containing noise for all of the gains $L_{out,i,j}$ is available. The actual illuminance has to be estimated from this data before the frames can be combined. The output of the frame with the highest gain that is not saturated will be used as an estimate of the actual illuminance at the pixel. Since this has an error because of noise, the used weights will not be completely optimal.

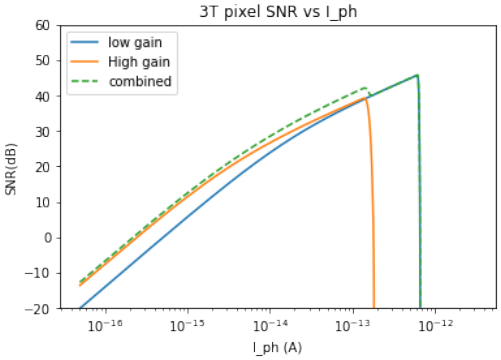

(A) SNR curve plotted against the photocurrent for the low gain mode, high gain mode and the combined HDR image SNR.

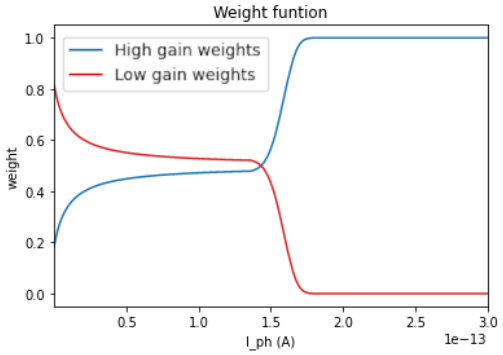

(B) Weights for optimal SNR with uncorrelated photon shot noise.

FIGURE 5.2: HDR merging with uncorrelated photon shot noise.

During the derivation of equation 5.2, the assumption was made that all the noise sources for the different gains are independent. This is not always the case. In some HDR implementations, the photon shot noise is for example the same in all the HDR frames since only one integration period has been done. Formula 5.2 can be updated to include the noise correlation as well (derivation in appendix B). The formula in the case of two gains is:

$$SNR_{total}(L_{in})^{-1} = w_0^2(L_{in})SNR_0(L_{in})^{-1} + w_1^2(L_{in})SNR_1(L_{in})^{-1} + 2w_0w_1\frac{cov(y_0, y_1)}{P_{signal}} \tag{5.3}$$

Here, the ideal weights can again be found using a brute force approach. The covariance could be calculated from the photo-response measurement data as well. Because the photon shot noise can no longer be averaged out, the SNR improvement will thus be less effective compared to the uncorrelated case. The weights for the same theoretical model, but this time with correlated photon shot noise, are plotted in figure 5.3. As can be seen there, there is almost no improvement in the SNR compared to binary weights (select the gain with the highest SNR for each

illuminance). Because of this, binary weights will be used when the photon shot noise is correlated.

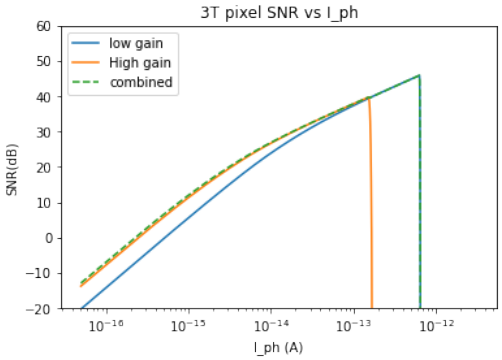

(A) SNR curve plotted against the photocurrent for the low gain mode, high gain mode and the combined HDR image SNR.

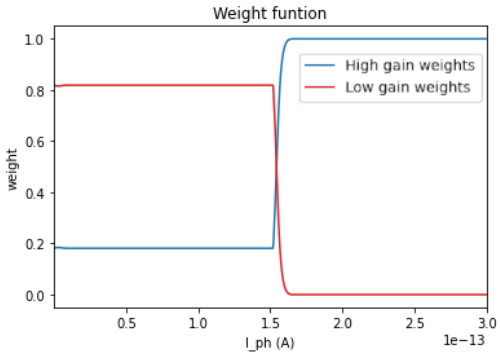

(B) Weights for optimal SNR with correlated photon shot noise.

Figure 5.3: HDR merging with correlated photon shot noise.

5.2 Image Artefacts

Even after the image correction, the response curves from the different gains of an HDR sensor are not completely linear. Thus, when using binary weights or when using a weight function that has a steep slope, there will be a step in the combined photo-response. An example from a real sensor is plotted in figure 5.4. This step will create artefacts in the merged HDR image. The easiest solution would be to increase the order of the non-linearity correction order to reduce the error between the photoresponse curves of the different gains (section 4.5), and thus reduce the step size.

It is not possible to correct the non-linearity completely, even when a high order correction is used. And sometimes, a higher order can require too much time to compute. In these cases it is necessary to smooth the weight function. The smoothness restriction will result in a lower SNR, thus a trade-off has to be made between artefacts and SNR.

To minimize the artefacts, the weight functions should have a steep slope where the error between the gains is small and a small slope when the error is large. The weights that create the smoothest transition are plotted in blue in figure 5.5. The slope of these weights is inversely proportional to the error between the gains. As can be seen from this, the weights should in this case rise quickly in the low illumination region. This is in contradiction to the optimal SNR weights where the steepest slope is near the saturation of the high gain response. To prevent the slope from becoming infinite when the error becomes zero at a certain point, the maximal slope can be limited. This is useful if, because of drift in the sensor characteristics, the point with

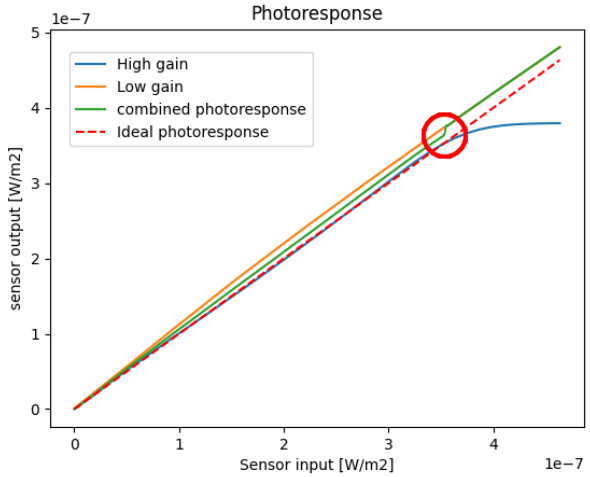

FIGURE 5.4: Step in combined photo response because of steep slope in weight function.

zero error would move somewhat.

To make a better trade-off between the artefacts and the SNR when binary weights would provide the optimal SNR, it is possible to calculate the optimal weights but move the starting point of the weights closer to the saturation point as is illustrated by the red curves in figure 5.5. This method is extended to image sensors with more than two different gains. The starting point depends on the actual error between the curves and the maximal acceptable artefacts.

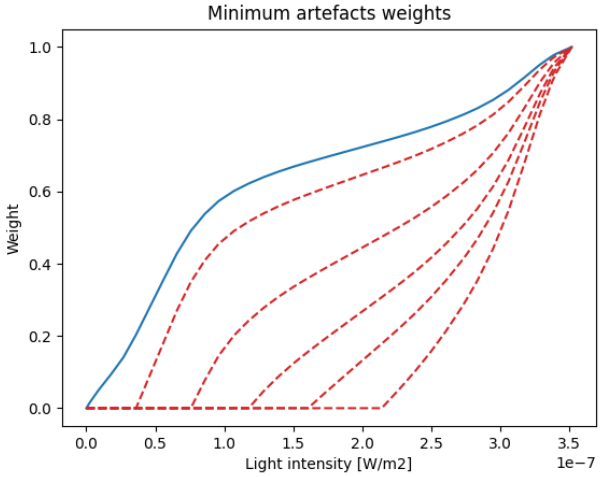

FIGURE 5.5: Weight function for minimal artefacts with different starting points.

5.2.1 Tone Mapping

The final exposure map needs more bits per pixel than the individual frames to store the information because of the increased dynamic range. Monitors often only have a resolution of around eight bit and cannot display the HDR scene. To solve this, tone mapping transforms the linear exposure map to something that can visualize the high dynamic range on monitors [16]. This has not been implemented in this thesis. There are several implementations in literature which often focus on what looks the best for humans.

5.3 Conclusion

A novel method to find the optimal weights is discussed in this chapter. The ideal weights for optimal SNR were tried first, but by using the calibration data instead of relying on a camera model. The idea of averaging out the noise does however no longer work for true HDR sensors, where binary weights provide the almost optimal SNR. Artefacts are created when using this function. A weight function that minimizes these artefacts has been proposed, but at the cost of a decreased SNR.

Chapter 6

Measurement Results on a Dual Gain HDR Sensor

The image correction and merging algorithms will be verified on a real image sensor in this chapter. The sensor used is a multiple capture HDR image sensor. This chapter will begin with a brief description of this sensor. Afterwards, the measurement procedure will be described and finally the results will be discussed when operating the sensor in global and rolling shutter.

6.1 Image Sensor Overview

This sensor is a front side illuminated HDR image sensor based on a 4T pixel. An extra overflow switch is connected to a storage capacitor to change the full well capacity. A schematic of the pixel is shown in figure 6.1. CDS is implemented to reduce the noise. It is theoretically possible to capture the low gain and high gain HDR frame from the same integration period using a three level TG method (section 3.4), but this was never implemented and tested in the control software for this sensor. For this reason, first an image with the overflow capacitor switch on and then another image with the overflow capacitor off have to be captured after each other to acquire the HDR frames. Both images will now be the result of a separate integration period.

The sensor can operate both in rolling and global shutter mode. In rolling shutter, the reset frame is subtracted on-chip and only one frame has to be read out. In global shutter, the reset values of all the pixels are read out first, and afterwards, the signal values of all the pixels are read out. An interleaved readout path is used to increase the speed (section 4.4). The internal gain of the readout path can be programmed to match the ADC range. The resolution of this sensor is 4096 by 4096 pixels. External ADCs are used, each connected to multiple columns, reading out a differential voltage at the output of the sensor. [34]

This sensor includes a test-row that can be enabled for characterization purposes.

This row includes sixteen identical blocks with each twenty EB4 black pixels and some gray-scale pixels, implemented as a resistor ladder [34].

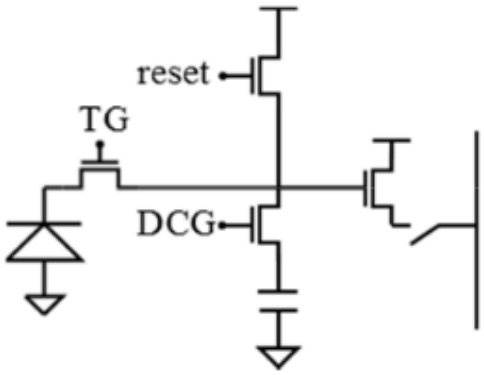

Figure 6.1: HDR pixel of the image sensor. Courtesy [28].

6.2 Measurement Setup

Figure 6.2 shows a picture of the measurement set-up for the photo-response measurement. The image sensor is mounted on a test board that can be remotely controlled by a computer. A Python framework is available to control all the test equipment. This set-up is placed in a dark cabinet and it should be taken care of that stray light cannot enter, especially at the entry point of the cables that connect the computer to the measurement equipment. It is also important to disable or cover all the indicator LED's on the electronics inside the dark cabinet.

An 830nm LED light source is used to illuminate the sensor (the wavelength is not important because this sensor has no color channels). The light intensity of these light sources can be temperature dependent, thus it is advised to wait for around ten minutes to allow the light source to stabilize before using the light source. It is also important that the illumination of the sensor is uniform. For this reason, the distance between the image sensor and the light source is made as large as possible and the image sensor is placed directly under the light source.

The light intensity can be controlled by setting a DAC value in the light source. The relation between this DAC value and the actual illumination of the sensor is not linear. A calibration has to be done for each set-up (because the actual illumination of the sensor depends on the distance between the light source and image sensor). To do this calibration. A reference diode is placed on the sensor or as close to it as possible. This reference diode is connected to a picoammeter that can be controlled by the computer as well. A sweep of the light source's DAC values is then done and the light intensity at the reference diode is measured for each step. These values can

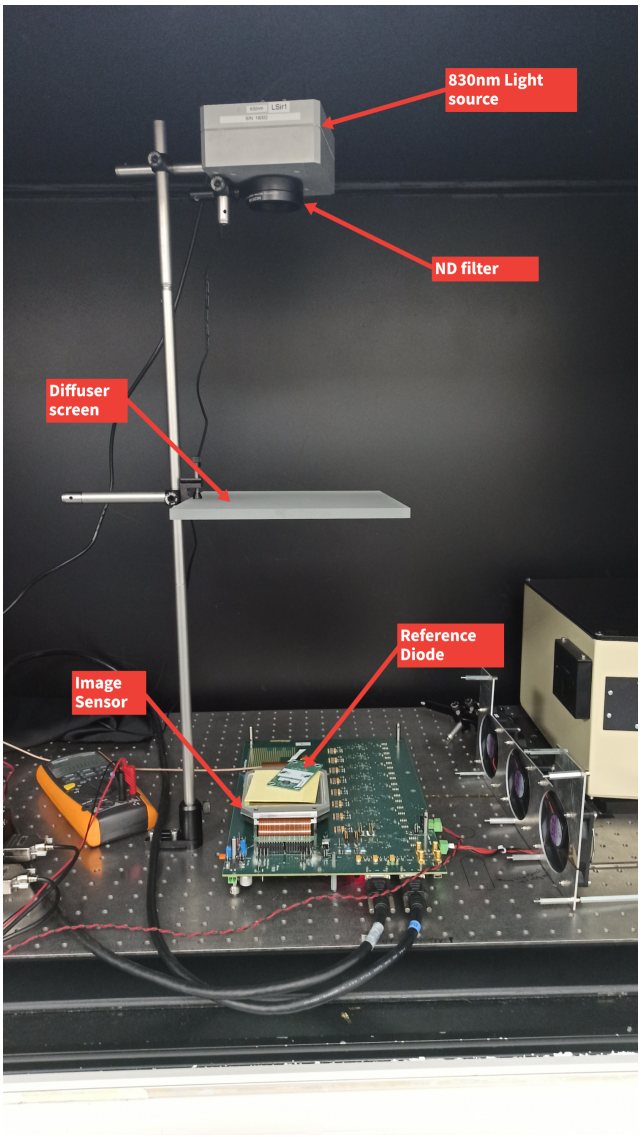

FIGURE 6.2: Measurement setup.

be interpolated later.

For this sensor, saturation happens at a low DAC value. This limits the resolution because the number of possible steps is limited. The amount of light actually reaching the sensor has to be reduced to increase the resolution. A neutral density filter (a filter that reduces the light intensity of all the wavelengths equally) with an optical density of one is used. This means that only 10% of the light passes through it. A diffuser plate is also placed between the light source and the sensor to block even more light and this also helps to create a more uniform illumination.

The output of the sensor is a differential voltage and the ADCs have a range between minus two and two volts. The reference voltage of the ADC has to be chosen as low as possible without clipping of the dark frames. After that, the gain of the readout chain is chosen so that there is no overflow of the ADC when the sensor is saturated. An internal gain of one was eventually used.

Finally, the performed photo response measurement is done by sweeping the light source DAC over fifty steps. For each illumination level, ten images are captured to determine the the average signal level and standard deviation. It is important that the sensor reaches saturation just before the highest DAC setting in the sweep because saturated frames contain no extra information and the whole photoresponse is required. It is also required to wait until the temperature of the image sensor is settled as well. Doing the measurements immediately from a cold start will result in a different dark current and dark current gradient.

For the dark current measurement, no light source is required. The sensor is placed in the dark cabinet and the sensor's light-sensitive area is covered to reduce the amount of stray light even more, because dark current measurements are sensitive to this stray light. The integration time is then varied between the minimal integration time (0,047s) and ten seconds, by doubling it every step. After the longest integration time, another image was taken with the minimum integration time to verify that the temperature has remained more or less constant during the measurement. It is again important for this measurement that the sensor has time to reach a nominal operating temperature before doing the measurement.

6.3 Results in Rolling Shutter

First, the procedure explained in the previous section has been done while operating the sensor in rolling shutter mode. In figure 6.3a, the average photoresponse curve for both the low gain and high gain modes are plotted before any correction has been done. Both curves show a steeper slope at low illumination levels compared to the medium illumination levels, which results in a non-linearity. The ideal linear photoresponse is also plotted in this figure to show the non-linearity error. The average dark current response curve for a varying integration time is plotted in figure 6.3b. This curve is almost linear in function of the integration time as expected, but shows a slight non-linearity for low integration times. Figure 6.3c shows the photon transfer curve for the temporal noise only. The low illumination part of both curves looks as expected, showing a flat region representing the readout noise dominated region and a linear slope, representing the photon shot noise dominated region. At high illumination however, the noise of the low gain curve becomes lower with increasing illumination. This should not be possible since the photon shot noise should be dominant in the high illumination region, and thus the total noise should increase relative to the sensors output level. The reason for this behaviour is not known. The high gain response does not show this behaviour and this issue appears in

the global shutter mode as well. Because the high gain response will be saturated for the light intensity where this occurs, this will not have an effect on the calculation of the HDR merging weights. The noise also has no effect on the non-linearity correction.

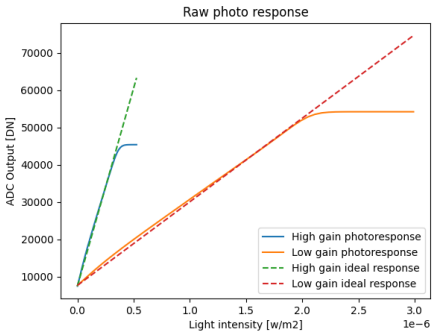

(A) Raw photoresponse and the ideal photoresponse for the low gain and high gain setting.

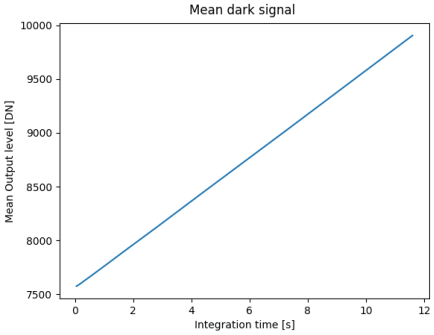

(B) Dark current for different integration times.

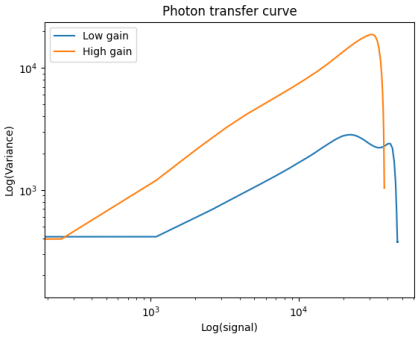

(C) Raw photon transfer curve for high and low gain.

FIGURE 6.3: Rolling shutter measurement results.

The corrected photoresponse after a third order correction can be seen in figure 6.5b and figure 6.5c, together with the interval that contains 95% of the pixel values. Since no temperature sensor or usable black pixels where present in this sensor, the dark current was estimated based on the integration time only with the assumption that the temperature remained constant. The average photoresponse is also plotted in these plots as the red dotted line. The response curve is more linear after the correction, as can be seen from this plot and from the 95% interval, more responses of the different pixels are uniform as well. After the saturation point, the corrected photoresponse is less uniform than before. The curves can now be directly used for HDR merging. No scaling of the low-gain curve is needed any more because equation 4.5 fits both the high gain and low curves to the actual light intensity at the input of the pixel.

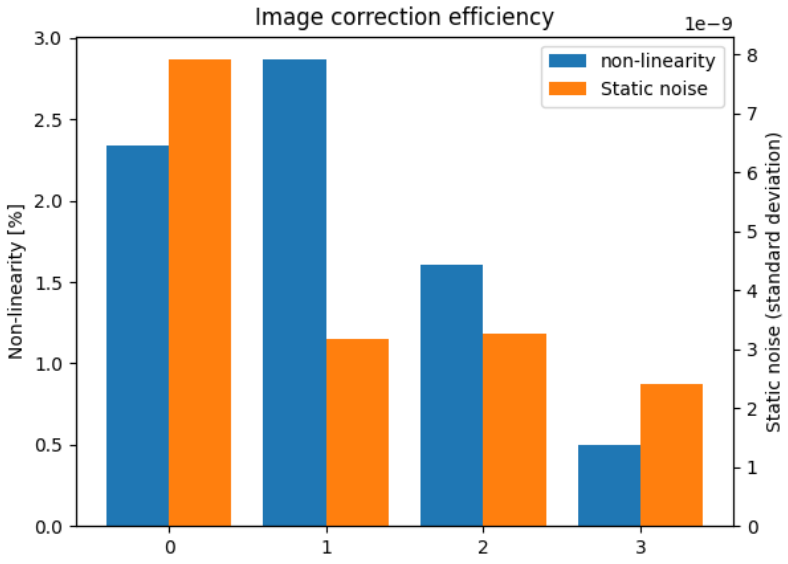

Figure 6.4: Static noise reduction for different correction algorithm orders.

The resulting static noise and non-linearity, calculated using equation 2.7, after corrections with different orders are shown in figure 6.4. The average noise is found by using a weighted average using the weight function described in section 4.6. As can be seen, a first order (PRNU correction only) improves the static noise a lot compared to using no correction at all. The non-linearity becomes even slightly larger. A second order does not create an improvement in static noise reduction in this case, but it makes the response more linear. A third order creates an even more linear response and reduces the static noise by a small amount as well.

The weights used for merging the gains are plotted in figure 6.6a. The low illumination part of this uses the optimal weights that average out noise (section 5.1), since the photon shot noise is uncorrelated in this sensor. The high illumination part uses the weights that result in the minimal amount of artefacts since the weights that provide optimal SNR have a steep slope in this area (section 5.2). To calculate the weights that result in minimal artefacts, the sensor is considered saturated when the corrected photoresponse deviates more than 2% from the ideal photoresponse. The merged photoresponse curve (after a third order correction) is plotted in figure 6.6b and, as can be seen in this graph, there is no step visible in the merged response. Finally, the SNR curves of both the gains and the merged SNR curve are plotted in figure 6.6c, showing the dynamic range improvement of the HDR method and the effect of using the noise averaging method on the SNR.

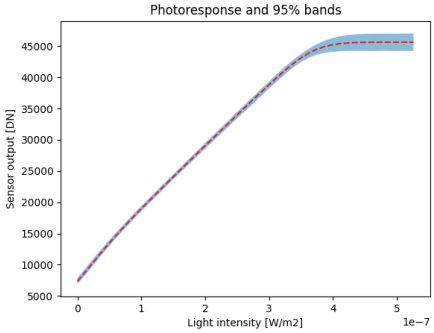

(A) Interval containing 95% of the pixels of the raw high gain response.

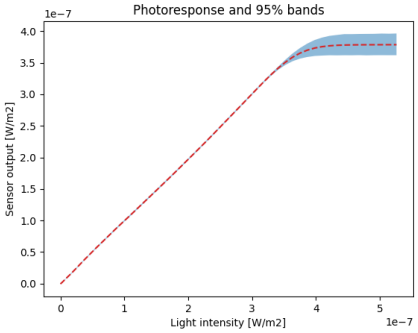

(B) Interval containing 95% of the pixels after correction of the high gain response.

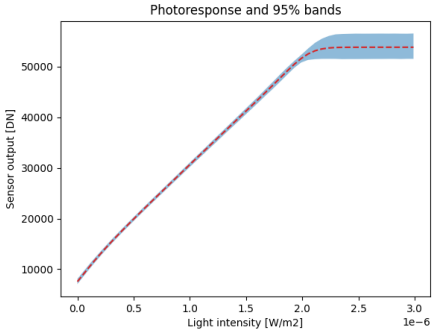

(C) Interval containing 95% of the pixels of the raw low gain response.

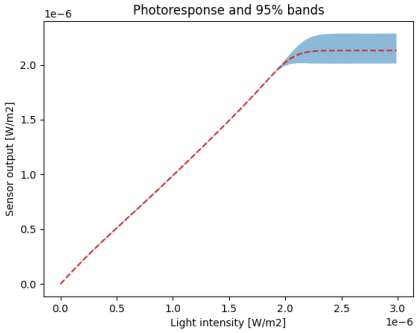

(D) Interval containing 95% of the pixels after correction of the low gain response.

FIGURE 6.5: Correction results.

6.4 Results in Global Shutter

The same measurement has been done while operating the sensor in global shutter mode to test the algorithm on an off-chip CDS sensor. The dark current in this mode is higher compared to the rolling shutter mode because of the extra dark current source at the FD current during the charge storage period. This extra dark current is much greater than the FD dark current [13], thus the average dark current can be be estimated by using the EB4 black pixels (section 4.3). These pixels have storage node dark current. The raw photoresponse is plotted in figure 6.7a. The sensor also has a greater non-linearity compared to the rolling shutter mode, with the slope of the photoresponse curve increasing near the saturation region. A third order correction is needed to achieve a linear response for this operation mode. As can be seen from the combined photorespones curve, plotted in figure 6.7c the photoreponse curve is linear after the third order correction and merging. The static noise is also reduced by almost a factor four.

The merging weights can be seen in figure 6.7b. These are almost the same as

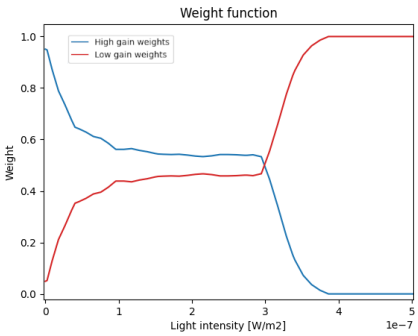

(A) Weight function used for HDR merging.

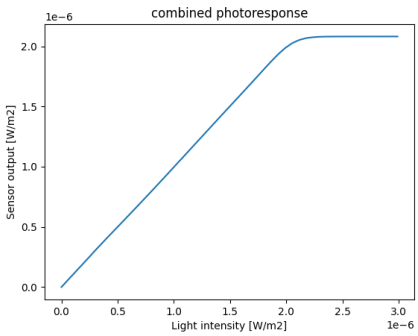

(B) combined photoresponse in rolling shutter mode.

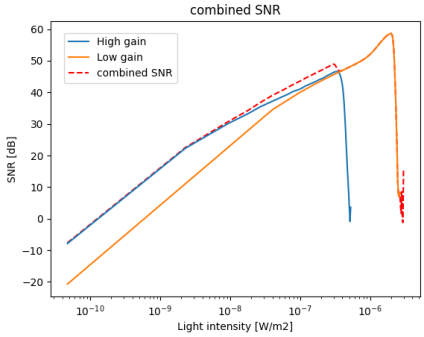

(C) SNR of the low gain, high gain and combined response.

Figure 6.6: HDR merging in rolling shutter.

the rolling shutter case because of the similar noise behaviour in this mode. The combined photoresponses show no step with the used weights. The dynamic range is increased 16.5 dB thanks to the multiple capture technique. Finally, the combined SNR is shown in figure 6.7d.

6.5 Conclusion

The methods explained in section 4 and section 5 are tested on this sensor in different operation modes. The third order corrections and the dark current estimation algorithm result in a reduced spatial noise, and a good linearity is achieved in both operating modes. The HDR frames also have to be merged into one frame without any artefacts and averaging out noise at the same time. The measurements did however show some irregularities (photon shot noise becoming lower with increased light intensity). These problems should have no influence on the image correction and merging algorithm itself.

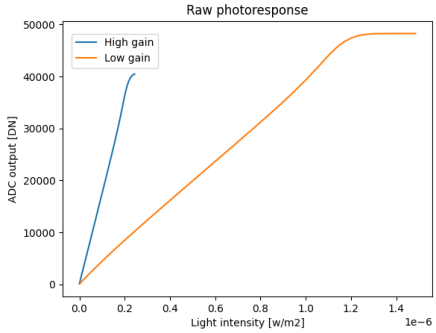

(A) Global shutter raw photoresponse.

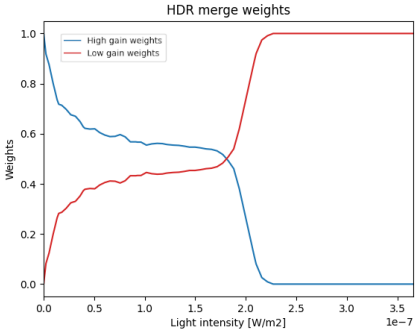

(B) Global shutter merging weights.

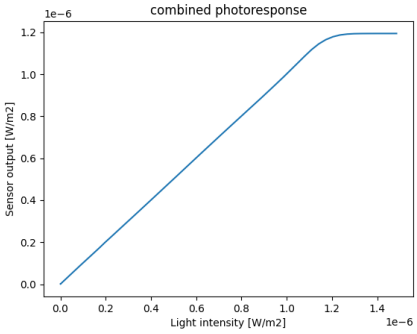

(C) HDR combined photoresponse in global shutter mode.

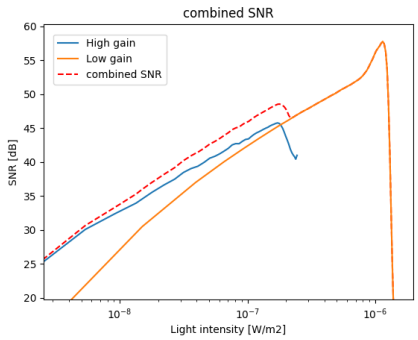

(D) Combined SNR in global shutter mode.

FIGURE 6.7: Global shutter measurement results.

Chapter 7

Measurement Results on a True HDR Global Shutter Image Sensor

The correction and HDR merging algorithm has also been tested on a true HDR sensor. First an overview of the sensor will be given. The measurement setup will be explained next. The most important results will be shown afterwards.

7.1 Image Sensor Overview

The pixel used is a 7T True HDR pixel that is optimized to operate in global shutter mode, and able to do integrate while read (IWR). The schematic of the pixel is shown in figure 7.1. During integration, EHP's are generated at the photodiode. The electrons that will not fit on the storage node will overflow over TG3 to a storage capacitor for later use during the integration. After the integration period, TG1 is opened and the remaining electrons on the PPD will move to the SN. During the readout, the charge on the storage node after TG1 is read out first using CDS, yielding the high gain frame. Afterwards, the merge switch is opened and the sum of the charge from both the storage nodes is read out, yielding the low gain frame. The readout path in this sensor uses an interleaved readout to increase the frame rate. Unlike the previous image sensor, this sensor is able to operate in true HDR mode, were both the low and high gain frames are read out from the same integration time. [20] [15]

7.2 Measurement Setup

The measurement set-up for the photoresponse and dark current is similar to the one used in chapter 6. The test system was placed in a dark cabinet and uniformly illuminated with a controllable light source. The photodiode was placed next to the image sensor instead to calibrate the light source. Because of the tall test system,

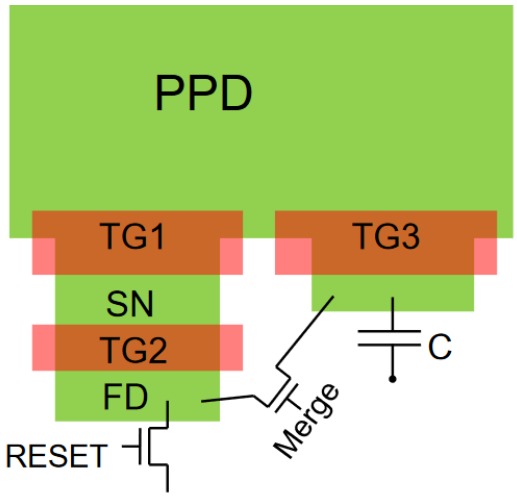

Figure 7.1: Global shutter HDR pixel. Courtesy [20].

the distance between the light source and the image sensor is smaller in this set-up. This test system heats up quickly, so the measurements had to be performed in a short timespan to avoid overheating the sensor and altering the dark current. A sweep of the DAC values of the ligth sources was done using 80 steps in total. 100 images at each step were taken to average out the noise and calculate the SNR. The steps were spaced closer to each other in the in the low illumination region for an increased resolution of the high gain response.

7.3 Results

figure 7.2a shows the photoresponse for both the low gain and the high gain frames. This measurement was stopped a little too early, before the saturation of the low gain occurred, because the light source reached the maximal level. A different wavelength should have been used. As can be seen in this figure, the photoresponse of this sensor has a neglectable non-linearity (smaller than 1%), so only a first order correction (PRNU only) was done in this case. The average dark current could again be estimated based on blocks of EB4 test pixels. The dark current in this sensor was a lot higher than the dark current in the previous sensor as well.

The HDR weights used for merging the frames are shown in figure 7.2b. The photon shot noise can not be averaged out, so the ideal weight is a step function, with smoothing to avoid artefacts. The starting point of the saturation weights was chosen at half the saturation illuminance. The combined photoresponse can be seen in figure 7.2c. The frames can be merged without artefacts in the transition region.

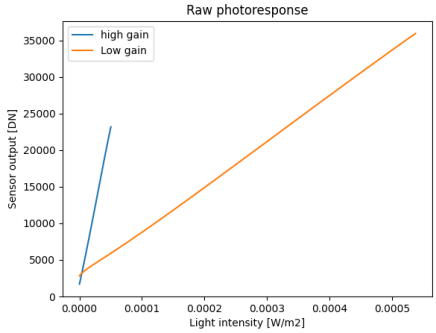

(A) Raw photorespons.e

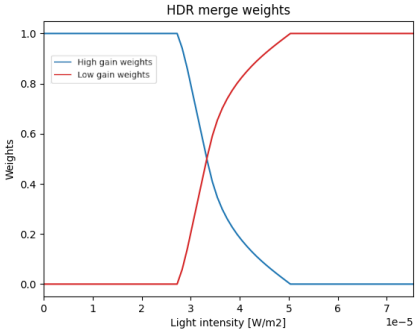

(B) Merging weights.

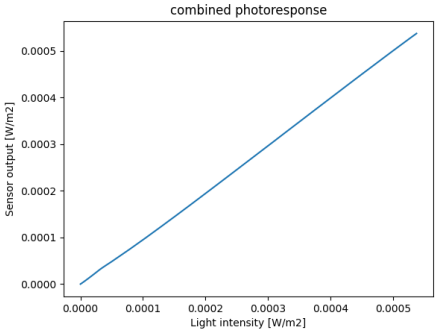

(C) Combined photoresponse.

FIGURE 7.2: Measurement results on a true HDR image sensor.

7.4 Conclusion

The correction and HDR merging algorithms have been tested on this image sensor as well. This sensor had a linear response, so only a first order correction was necessary. The photon shot noise could not be averaged out on this sensor, so a weight function that limits the artefacts has been used. The photoresponse measurement was stopped too early because the light source was saturated. This has no influence on the merging of the images.

Conclusion

A calibration based image correction was proposed first. The method identifies all the noise sources in a CMOS image sensor, and corrects them individually in the correct order. First the offset in each column is subtracted from the sensor output, next a polynomial correction of the non-linearity for each pixel's response is performed. The order can be changed depending on the image sensors initial non-linearity, but a second or third order will be sufficient in most cases. The polynomial interpolation also helps to reduce the static noise.

Next, the dark current has to be corrected. This is done based on the idea that the average dark current can be estimated based on the black test pixels, which are often present in Caeleste image sensors. The advantage of this is that the correction method is resistant to a change in operating conditions. A dark current image can then be scaled linearly based on the black pixel average. The disadvantage of this method is that black pixels are required, and not all types of black pixels are suitable. Ideally, EB0 pixels should be used. EB4 pixels can be used as well when the PPD dark current is not dominant to approximate the average dark current, but this will result in a small error. The temperature behaviour of black pixels is not linear but exponential, this will also result in an error when the sensor has a large temperature deviation compared to when the calibration was done. A temperature gradient in the image sensor will also decrease the accuracy of this method.

Finally, the frames of the different gains have to be merged into one HDR image. A method to do this with minimal noise has been proposed. The merging weights can be found directly from the calibration data. This is however not effective on true HDR sensors, where the photon shot noise can no longer be averaged out. In that case, binary weights should be used to achieve an optimal SNR. This creates artefacts, and a smoother weight function is used in practice, where the slope depends on the error between the photoresponse curves of the different gains after correction. This comes at the cost of a reduced SNR at the transition region.

The performance of this algorithm has been verified on two different image sensors. The images have been corrected successfully on both sensors, showing a reduced static noise and a non-linearity below 1% could be achieved on both sensors. The HDR frames could also be merged without showing artefacts. The measurements did show some problems. On the first sensor, the noise was decreasing with in-

creasing illumination. On the second sensor, the photoresponse measurement was stopped too early. These problems should however have no influence on the algorithm.

A calibration has to be performed to get the required parameters, and these calibrations have to be done in a lab-environment. This means that this method is in practice best used for high performance image sensors, where the effort of doing this calibration is less problematic. All the operations needed for the correction are linear, so they could be implemented efficiently, and the correction could be done in real time, immediately after capturing each image. An FPGA implementation could also be implemented doing these corrections before any data is sent to a computer.

Appendices

Appendix A

Combined SNR

Suppose an image sensor produces n frames with a different gain that have to be combined into a HDR frame. The outputs y_i of these gains for a pixel, after correcting all the non-linearities and static noise sources, consists of a signal part S and a noise part N_i:

$$\begin{cases} y_0 = S + N_0 \\ y_1 = S + N_1 \\ \vdots \\ y_n = S + N_n \end{cases} . \tag{A.1}$$

These can be combined to find the value of the pixel in the HDR image using a weight function:

$$y_{combined} = \sum_{i=0}^{n} w_i y_i \text{ where: } \sum_{i=0}^{n} w_i = 1 \tag{A.2}$$

The SNR of this signal can be found as:

$$SNR_{combined} = \frac{E[y_{combined}^2]}{var(y_{combined}} \tag{A.3}$$

Where the signal power can be calculated as:

$$E[y_{combined}^2] = P_{signal} = S^2 \tag{A.4}$$

Because it is the same for all signals and the noise is assumed to have an average of zero. The noise power can be found as:

$$var(y_{combined}) = var(\sum_{i=0}^{n} w_i y_i) \tag{A.5}$$

$$= var(\sum_{i=0}^{n} w_i N_i) \quad \text{Signal is constant.} \tag{A.6}$$

$$= \sum_{i=0}^{n} var(w_i N_i) \quad \text{Assume all noise sources independant.} \tag{A.7}$$

$$= \sum_{i=0}^{n} w_i^2 var(N_i) \tag{A.8}$$

Using these equations, the combined SNR can be found as:

$$SNR_{combined} = \frac{E[S^2]}{\sum_{n=0}^{n} w_i var(N_i)} \tag{A.9}$$

$$= \left[\frac{\sum_{n=0}^{n} w_i^2 var(N_i)}{E[S^2]} \right]^{-1} \tag{A.10}$$

$$= \left[\sum_{n=0}^{n} w_i^2 SNR_i^{-1} \right]^{-1} \tag{A.11}$$

Appendix B

Combined SNR With Correlated Noise

In appendix A, the noise sources were assumed independent. If this is not the case, the combined noise in the case of two gains ca be found as:

$$var(y_{combined}) = var(w_0 y_0 + w_1 y_1) \tag{B.1}$$

$$= w_0^2 var(y_0) + w_1^2 var(y_1) + 2 w_0 w_1 cov(y_0, y_1) \tag{B.2}$$

From this, the combined SNR can be found again as:

$$SNR_{combined} = \frac{S^2]}{var(y_{combined})} \tag{B.3}$$

$$= \frac{S^2]}{w_0^2 var(y_0) + w_1^2 var(y_1) + 2 w_0 w_1 cov(y_0, y_1)} \tag{B.4}$$

$$= \left[\frac{w_0^2 var(y_0) + w_1^2 var(y_1) + 2 w_0 w_1 cov(y_0, y_1)}{S^2} \right]^{-1} \tag{B.5}$$

$$= \left[w_0 SNR_0^{-1} + w_1 SNR_1^{-1} + \frac{2 w_0 w_1 cov(y_0, y_1)}{S^2} \right]^{-1} \tag{B.6}$$

Bibliography

[1] Best practice 31. Caeleste BVBA internal documentation.

[2] Course on noise. Caeleste BVBA internal documentation.

[3] Stpython documentation. Caeleste BVBA internal documentation.

[4] What are global shutter and rolling shutter? how to choose the one that fits the application? https://www.e-consystems.com/blog/camera/technology/what-are-global-shutter-and-rolling-shutter-how-to-choose-the-one-that-fits-the-appli Accessed: 2022-05-06.

[5] What is a backside illumination cmos sensor? https://www.nikonimgsupport.com/eu/BV_article?articleNo=000006485&configured=1&lang=en_GB. Accessed: 2022-06-05.

[6] A novel method to increase linlog cmos sensors's performance in high dynamic range scenarios. Sensors, 2019.

[7] Cmos image sensor industry: Huawei ban reorders the player growth ranking. http://www.yole.fr/Status_Of_CMOS_Image_Sensor_Industry_MarketUpdate_Yole_August2021.aspx, 2021. Accessed: 2022-06-01.

[8] Emva standard 1288 standard for characterization of image sensors and cameras, release 4.0 general, 6 2021.

[9] Emva standard 1288 standard for characterization of image sensors and cameras, release 4.0 linear, 6 2021.

[10] A. Abarca, S. Xie, J. Markenhof, and A. Theuwissen. Integration of 555 temperature sensors into a 64 x 192 cmos image sensor. Sensors and Actuators A: Physical, 2018.

[11] ajing Zheng, L. Zheng, Z. Yu, B. Shi, Y. Tian, and T. Huang. High-speed image reconstruction through short-term plasticity for spiking cameras. IEEE Conference on Computer Vision and Pattern Recognition, 2021.

[12] R. C. C. alik, E. Tunali, B. Ercan, and S. Oz. A study on calibration methods for focal plane array cameras. International Conference on Computer Vision Theory and Applications, 1 2018.

[13] J. Basteleus. T8 test report. 8 2018.

[14] N. Blanc. Ccd versus cmos-has ccd imaging come to an end?, 2003.

[15] G. Cai1, K. Tajima, A. V. Hoorebeeck, P. Stampoglis, B. Luyssaert, B. Dierickx, C. Gokel1, T. V. Uffelen, G. Ruttens, J. Yamane, and I. Ishii. A 1.3m pixel 34,700fps global-shutter bsi imager with hdr and motion blur suppression capability. https://caeleste.be/wp-content/uploads/2021/10/P16_Cai-presentation.pdf, 2019. Accessed: 2022-05-31.

[16] A. Darmont. *High dynamic range imaging : sensors and architectures*. SPIE, second edition, 3 2019.

[17] S. Decker, D. McGrath, K. Brehmer, and C. G. Sodini. A 256 256 cmos imaging array with wide dynamic range pixels and column parallel digital outp. EEE Journal Of Solid-State circuits, 1998.

[18] B. Dierickx. High dynamic range the pixel standpoint. ISSCC Forum on Image sensors, 2 2008.

[19] B. Dierickx. Imperfections of high-performance image sensors. Lorentz Workshop, 2015.

[20] B. Dierickx, A. Kalgi, D. V. Aken, A. Klekachev, J. Basteleus, P. Stampoglis, G. D. Nicolantinio, F. Palumbi, and A. Pelamatti. A rad-hard, global shutter, true hdr, backside illuminated image sens. Space and scientific CMOS image sensors workshop, 2019.

[21] I. Dinstein, F. Merkle, T. Lam, and K. Wong. Imaging system response linearization and shading correction. IEEE International Conference on Robotics and Automation, 1984.

[22] F. Dufaux, R. K. Mantiuk, P. L. Callet, and M. Mrak. *High Dynamic Range Video: From Acquisition, to Display and Applications*. Elsevier, 2016. Pages 85-119.

[23] J. C. Dunlap, E. Bodegom, and R. Widenhorn. Correction of dark current in consumer cameras. Journal of electronic imaging, 2010.

[24] D. Durini, M. Deans, K. D. Santos, J. Leonard, and S. Pazhayattil, editors. *High Performance Silicon Imaging Fundamentals and Applications of CMOS and CCD Sensors*. Elsevier, 2020.

[25] W. Fei. *Linearity Research of a CMOS Image Sensor*. PhD thesis, 2018.

[26] A. E. Gamal. High dynamic range image sensors. https://cafe.stanford.edu/~abbas/group/papers_and_pub/isscc02_tutorial.pdf. Accessed: 2022-01-10.

[27] M. Granados, B. Ajdin, M. Wand, C. Theobalt, H.-P. Seidel, and H. P. A. Lensch. Optimal hdr reconstruction with linear digital cameras. Computer Society Conference on Computer Vision and Pattern Recognition, 2010.

[28] A. K. Kalgi, B. Dierickx, B. Dupont, P. Coppejans, B. S. P. Gao, B. Luyssaert, A. Defernez, J. Zhu, J. Basteleus, W. V. Q. Yao, D. Uwaerts, B. Uwaerts, G. Ruttens, and G. Cai. Four concepts for synchronous, psn limited, true cds, hdr imaging. International Image Sensor Workshop, 2015.

[29] J.-P. Kong and S.-J. Lee. Ccd signal processing for optimal non-uniformity correction. Korean Journal of Remote Sensing, 2010.

[30] A. Krymski. Types of charge-coupled devices with their working principles. https://www.elprocus.com/know-about-the-working-principle-of-charge-coupled-device/. Accessed: 2022-06-10.

[31] A. Krymski. Imlementing global shutter in a 4t pixel. IISS, 2009.

[32] L.-W. Lai, C.-H. Lai, , and Y.-C. King. A novel logarithmic response cmos image sensor with high output voltage swing and in-pixel fixed-pattern noise reduction. IEEE Sensors Journal, 2004.

[33] M. R. Lovejoy and M. A. Wickert. Testing an improved gain equalization non-uniformity correction algorithm. IEEE Radar Conference, 2013.

[34] B. Luyssaert, P. Gao, B. Dierickx, J. Basteleus, and A. Keefe. Large area low noise image sensor for electron beam microscope. 11 2018.

[35] B. C. Madden. Extended intensity range imaging. https://repository.upenn.edu/cis_reports/248, 1993. Accessed: 2022-04-11.

[36] S. Mahatoa, G. Meynantsb, G. Raskina, J. D. Riddera, and H. V. Winckel. Noise optimization of the source follower of a cmos pixel using bsim3 noise model. SPIE Astronomical Telescopes + Instrumentation, 7 2016.

[37] S. Mann and R. Picard. On being undigital with digital cameras: Extending dynamic range by combining differently exposed pictures. Technical Report 323, M.I.T. Media Lab Perceptual Computing Section, Boston, Massachusetts, 1994.

[38] T. Mertens, J. Kautz, and F. V. Reeth. Exposure fusion. Conference on Computer Graphics and Applications, 2007.

[39] T. Mitsunaga and S. Nayar. Radiometric self calibration. International Conference on Computer Science and Software Engineering, 2008.

[40] A. E. Mudau, C. J. Willers, D. Griffith, and F. P. J. le Roux. Non-uniformity correction and bad pixel replacement on lwir and mwir images. IEEE Electronics, Communications and Photonics Conference, 2011.

[41] D. Park, J. Rhee, and Y. Joo. A wide dynamic-range cmos image sensor using self-reset technique. IEEE Electron Device Letters, 2007.

[42] A. Pelamatti. Estimation and modeling of key design parameters of pinned photodiode cmos image sensors for high temporal resolution applications, 2015.

[43] M. Rozkovecand and J. Cech. Polynomial based nuc implemented on fpga. IEEE 2016 Euromicro Conference on Digital System Design (DSD), 2016.

[44] M.-K. L. Simon M. Sze. Semiconductor devices: Physics and technology, 5 2003.

[45] P. Stampoglis, A. Klekachev, A. K. Kalgi, D. Gautam, D. V. Aken, and D. Uwaerts. Elfis test report. 3 2020.

[46] N. Teranishi. The pinned photodiode, 6 2016.

[47] T. Toczek, F.Hamdi, B.Heyrman, J.Dubois, J.Miteran, and D.Ginhac. Scene-based non-uniformity correction: From algorithm to implementation on a smart camera. IEEE Journal of Systems Architecture, 2013.

[48] S. N. Torres, E. M. Vera, R. A. Reeves, and S. K. Sobarzo. Adaptive scene-based non-uniformity correction method for infrared-focal plane arrays. Proceedings of SPIE - The International Society for Optical Engineering, 2003.

[49] R. Widenhorn and M. M. Blouke. Temperature dependence of dark current in a ccd. Proceedings of SPIE, 2002.

[50] R. Widenhorn, J. C. Dunlap, and E. Bodegom. Exposure time dependence of dark current in ccd imagers. IEEE Transactions on Electron Devices, 2010.

[51] T. Willassen, J. Solhusvik1, R. Johansson, S. Yaghmai, H. Rhodes, S. Manabe, D. Mao, Z. Lin, D. Yang, O. Cellek, E. Webster, S. Ma, and B. Zhang. A 1280x1080 4.2um split-diode pixel hdr sensor in 110nm bsi cmos process. https://www.imagesensors.org.

[52] Y. Xu. *Fundamental Characteristics of a Pinned Photodiode CMOS Pixels*. PhD thesis, 2015.